

# LogoSP: Local-global Grouping of Superpoints for Unsupervised Semantic Segmentation of 3D Point Clouds

Zihui Zhang<sup>1,2†</sup> Weisheng Dai<sup>1,2†</sup> Hongtao Wen<sup>1,2</sup> Bo Yang<sup>1,2\*</sup>

<sup>1</sup> Shenzhen Research Institute, The Hong Kong Polytechnic University

<sup>2</sup> vLAR Group, The Hong Kong Polytechnic University

zihui.zhang@connect.polyu.hk, bo.yang@polyu.edu.hk

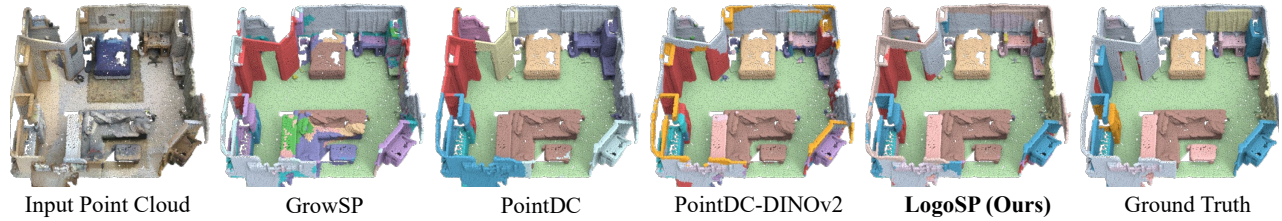


Figure 1. Given an input point cloud with complex structures from ScanNet dataset, our LogoSP automatically discovers accurate semantic classes such as *sofa* and *table* without needing human labels in training, clearly outperforming all existing baselines.

## Abstract

We study the problem of unsupervised 3D semantic segmentation on raw point clouds without needing human labels in training. Existing methods usually formulate this problem into learning per-point local features followed by a simple grouping strategy, lacking the ability to discover additional and possibly richer semantic priors beyond local features. In this paper, we introduce **LogoSP** to learn 3D semantics from both local and global point features. The key to our approach is to discover 3D semantic information by grouping superpoints according to their global patterns in the frequency domain, thus generating highly accurate semantic pseudo-labels for training a segmentation network. Extensive experiments on two indoor and an outdoor datasets show that our LogoSP surpasses all existing unsupervised methods by large margins, achieving the state-of-the-art performance for unsupervised 3D semantic segmentation. Notably, our investigation into the learned global patterns reveals that they truly represent meaningful 3D semantics in the absence of human labels during training. Our code and data are available at <https://github.com/vLAR-group/LogoSP>

## 1. Introduction

Semantic segmentation of 3D point clouds is crucial for a variety of emerging applications such as robot planning, embodied AI, and autonomous driving. To learn

per-point 3D semantics, early works focus on developing fully or weakly supervised techniques including 3D point-based [22, 25, 54] methods and 2D/3D projection-based approaches [16, 77]. While achieving remarkable accuracy and efficiency on public datasets, they predominantly depend on large-scale human annotations of raw point clouds for training neural networks. Unfortunately, the process of annotating 3D point clouds is particularly costly and labour-intensive. To mitigate this issue, an increasing number of recent works leverage supervised pretrained 3D, 2D/language features such as CLIP [56] and SAM [30], followed by finetuning techniques to learn per-point semantics. Despite yielding promising results, these methods still need tedious human annotations or alignments between modalities.

Very recently, several works tackle 3D semantic segmentation without needing human labels in training, including the seminal GrowSP [91], PointDC [8], and others [37, 45, 61, 72, 92]. By creating and then progressively growing 3D superpoints within raw point clouds, GrowSP successfully learns semantically meaningful primitives, ultimately achieving purely unsupervised 3D semantic segmentation. Nevertheless, the segmentation performance is still unsatisfactory. The primary reasons are two-fold. First, during its initialization stage, the per-point or per-superpoint features of GrowSP are often not sufficiently discriminative, as its backbone network is randomly initialized without incorporating semantic priors. Second, the latter strategy of grouping 3D superpoints is too simplistic, thus generating inferior pseudo-labels to train the network.

With the advancement of self-supervised pretraining

\* Corresponding author    † Equal contribution

techniques in 2D domain, semantic hints emerge from pre-trained features such as DINO/v2 [5, 46] in the absence of any human label during training. In this context, another unsupervised method PointDC [8] distills these self-supervised 2D features into 3D point clouds, followed by supervoxel grouping for estimating semantics. However, the supervoxel clustering process is error-prone and the resulting soft pseudo-labels often lack accuracy for training the network, which ultimately leads to inferior segmentation performance on 3D point clouds.

In this paper, we aim to advance the field of unsupervised 3D semantic segmentation. Building on the strengths of prior works, such as GrowSP [91] and PointDC [8], while tackling their limitations, we present a simple yet effective pipeline for achieving highly accurate 3D semantic segmentation without needing human annotations in training. Particularly, our pipeline comprises three major ingredients: 1) a 2D-to-3D distillation module that obtains preliminary but high-quality per-point features from self-supervised pre-trained models; 2) a bottom-up superpoint growing module that groups raw 3D points into superpoints based on local feature similarity; and 3) a top-down semantic pseudo-label generation module that aggregates superpoints into semantic elements. By constructing a global superpoint graph, this module groups superpoints based on their global features in the frequency domain after applying Graph Fourier Transform. The core of our approach lies in an effective combination of the latter two ingredients, which enables our pipeline to precisely learn per-point semantics through **local-global** grouping of superpoints without relying on human labels. We name our method **LogoSP** and Figure 1 shows qualitative results for an indoor 3D scene. Our contributions are:

- We advance the unsupervised semantic segmentation of 3D scene point clouds, seamlessly incorporating self-supervised pretrained 2D features.
- We present an effective technique for top-down grouping superpoints into semantic pseudo-labels based on superpoint features in the global frequency domain.
- We empirically demonstrate the effectiveness of LogoSP on various datasets, showing significant improvements over all previous unsupervised methods.

## 2. Related Works

**Fully-supervised 3D Semantic Learning:** In the past years, there has been tremendous progress in 3D semantic segmentation of point clouds. Current methods can be categorized into four main types: 1) point-based methods [18, 22, 23, 31, 36, 41, 55, 64, 70, 71, 75, 78, 93], which primarily follow the pioneering work PointNet [54] to learn per-point features via shared MLPs; 2) 3D voxel-based approaches [11, 34, 43, 51, 95], which follow the successful SparseConv [16] to project raw point clouds into reg-

ular grids followed by traditional 3D convolutional neural networks; 3) superpoint-based approaches [33, 59] which partition the 3D scene into more compact superpoints and assign segmentation results to each superpoint; and 4) 2D projection-based methods [32, 44, 77], which project point clouds onto 2D views and leverage established 2D neural architectures. Additionally, the advancement of self-supervised pretraining techniques developed for 3D domain [7, 21, 26, 49, 57, 74, 81, 86, 89] further enhances segmentation. While achieving impressive results, they rely heavily on human annotations which are prohibitively expensive.

**Weakly-supervised 3D Semantic Learning:** To alleviate the burden of human labeling, a line of works has been proposed to learn 3D semantics using sparser or cheaper annotations such as fewer 3D point labels [25, 39, 42, 66, 73, 79, 88] or patch-based labels [9, 38, 76]. By further leveraging self-supervised pretraining techniques for point clouds followed by supervised finetuning, many methods [21, 81, 89, 90] have obtained encouraging results. However, they still require human annotations and the trained models are often not generalizable to novel 3D scenes.

**Distilling Supervised 2D Features to 3D:** Recently, an increasing number of large 2D vision and/or language models have been developed including SAM/v2 [30, 58] and CLIP [56]. Thanks to large-scale 2D datasets with human labels and/or paired language descriptions, these models can extract high-quality visual features from 2D images. Based on them, a series of works [6, 14, 17, 19, 29, 35, 40, 47, 52, 53, 60, 69, 80, 82–85, 94] have been developed to project 2D features into 3D point clouds, yielding promising results for close/open-vocabulary 3D semantic learning. However, these methods fundamentally rely on human labels in 2D or language domains, making them less appealing for applications. In contrast, our method learns 3D semantics without any human labels.

**Unsupervised 2D/3D Semantic Learning:** For unsupervised semantic segmentation on 2D images, a number of works have been proposed to learn latent semantic representations by clustering per-pixel features, including the early DeepCluster [4], IIC [27], PiCIE [10], and many recent variants [15, 20, 28, 48, 65, 87]. Although achieving encouraging performance on 2D datasets, few methods show successful applicability in 3D space due to the domain gap between images and point clouds as demonstrated in [91]. For unsupervised 3D semantic learning, early works [63, 67] attempt to learn point semantics by recovering voxel positions or canonicalization, but they are limited to object-level point clouds. Very recently, the seminal GrowSP [91] and PointDC [8] demonstrated encouraging segmentation results on complex real-world 3D datasets without needing any type of human labels in training. In this paper, our new method surpasses them by large margins via effectively grouping superpoints of raw point clouds.

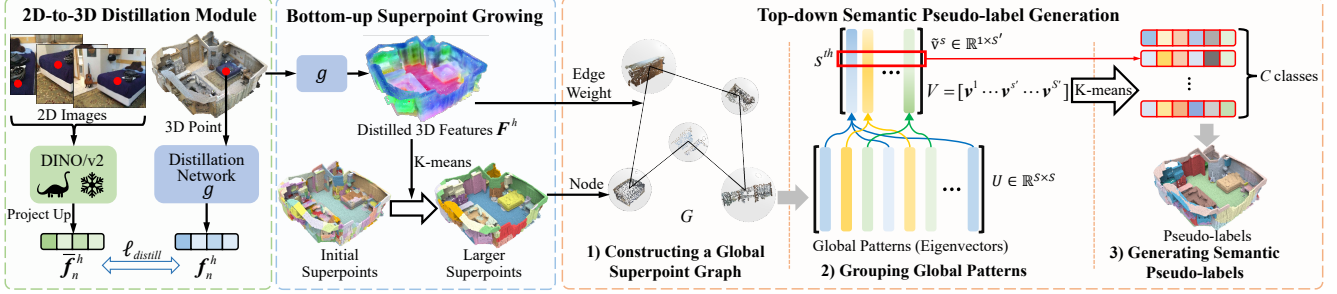


Figure 2. The framework of LogoSP. The leftmost block shows the 2D-to-3D distillation module, the middle block illustrates the bottom-up superpoint growing module, and the rightmost block describes all three steps of our top-down semantic pseudo-label generation module.

### 3. LogoSP

Given a dataset with  $H$  scene point clouds  $\{P^1 \dots P^H \dots P^H\}$ , for a specific  $h^{th}$  scene point cloud, we have  $N$  points, i.e.,  $P^h \in \mathbb{R}^{N \times 6}$ , where each point has a location  $xyz$  with color  $rgb$ . In the meantime, we also have  $K$  RGB/D images  $\{I_1^h \dots I_k^h \dots I_K^h\}$  associated with the  $h^{th}$  point cloud. Such 2D-3D aligned datasets can be easily collected in reality thanks to the wide availability of calibrated 2D/3D scanners on mobile devices or robots. Our goal is to estimate a semantic class belonging to  $C$  categories for any  $n^{th}$  point  $p_n^h$  in  $P^h$ . In practice, we may safely assume that the total number of semantic classes  $C$  is known, as indoor or outdoor scenes often comprise commonly interested classes.

#### 3.1. 2D-to-3D Distillation Module

As shown in the leftmost block of Figure 2, following PointDC [8], this module aims to leverage the self-supervised pretrained model in 2D domain to distill semantic priors to 3D. Particularly, given pretrained DINO/v2 [5, 46], for a specific point cloud  $P^h$  and its associated 2D images  $\{I_1^h \dots I_k^h \dots I_K^h\}$ , the distillation module has 3 steps:

**Step 1:** We feed all  $K$  images into the pretrained model, obtaining per-pixel features. Following the projection strategy of OpenScene [52], these 2D features are projected up to 3D space with the aid of depth images. For every point in  $P^h$ , if it has multiple feature vectors accumulated, we simply average them out; if it has no feature vector, that point will not be supervised in the subsequent Step 2.

**Step 2:** After the above Step 1, for a specific 3D point  $p_n^h$ , we have its final projected features  $\tilde{f}_n^h$ . Now, we train a SparseConv [16] from scratch as a distillation network  $g$  to regress the projected features for each 3D point. Following OpenScene [52], this 3D distillation net takes a single point cloud  $P^h$  as input and is supervised by the following loss:

$$\ell_{distill} = 1 - \cos(f_n^h, \tilde{f}_n^h), \quad f_n^h, \tilde{f}_n^h \in \mathbb{R}^{384} \quad (1)$$

where  $\tilde{f}_n^h$  is the predicted 3D features from SparseConv.

**Step 3:** We obtain a new 3D feature vector for every 3D point in the whole dataset (training split) through the well-trained distillation network  $g$ . Such 3D features tend to encode more spatial information in addition to semantic priors

inherited from 2D images. We reuse the trained network  $g$  in subsequent operations.

#### 3.2. Bottom-up Superpoint Growing

For a specific point cloud  $P^h$ , we now have its distilled 3D features  $F^h \in \mathbb{R}^{N \times 384}$  from net  $g$ . In this module, we aim to group raw 3D points into larger and larger superpoints that are likely to encode more and more semantic information. As shown in the middle block of Figure 2, following GrowSP [91], we summarize the steps as follows:

**Step 1:** We create a total number of  $M^0$  initial superpoints  $\{\tilde{p}_1^h \dots \tilde{p}_{m^0}^h \dots \tilde{p}_{M^0}^h\}$  for a point cloud  $P^h$ . Note that,  $M^0$  is actually different across different scenes.

**Step 2:** We compute mean features for all initial superpoints, denoted as  $\{\tilde{f}_1^h \dots \tilde{f}_{m^0}^h \dots \tilde{f}_{M^0}^h\}$ :

$$\tilde{f}_{m^0}^h = \frac{1}{Q} \sum_{q=1}^Q f_q^h, \quad f_q^h \in \mathbb{R}^{384} \quad (2)$$

where  $Q$  is the total number of 3D points within an initial superpoint  $\tilde{p}_{m^0}^h$ , and  $f_q^h$  is the feature vector retrieved from  $F^h$  for the  $q^{th}$  3D point of the superpoint.

**Step 3:** With these initial superpoint features, we use K-means to group the  $M^0$  vectors into  $M^1$  clusters, where  $M^1 < M^0$ . Each cluster becomes a new and larger superpoint. All new superpoints are:

$$\{\tilde{p}_1^h \dots \tilde{p}_{m^1}^h \dots \tilde{p}_{M^1}^h\} \xleftarrow{\text{K-means}} \{\tilde{f}_1^h \dots \tilde{f}_{m^0}^h \dots \tilde{f}_{M^0}^h\} \quad (3)$$

With the above three steps, we will have the following larger superpoints in Eq 4 for the whole dataset, and then they are all fed into our third component elaborated in Section 3.3, generating semantic pseudo-labels to continue training the network  $g$  (or a randomly initialized SparseConv) for a predefined  $E$  epochs, i.e., one round.

$$\{\{\tilde{p}_1^1 \dots \tilde{p}_{m^1}^1 \dots \tilde{p}_{M^1}^1\} \dots \{\tilde{p}_1^H \dots \tilde{p}_{m^1}^H \dots \tilde{p}_{M^1}^H\}\} \quad (4)$$

After one round, we will calculate the next level of larger superpoints by repeating Steps 2/3. Given  $T$  rounds of growth, the number of superpoints for an input point cloud will be decreased from  $M^1 \rightarrow M^2$  to a small value  $M^T$ . For simplicity, we follow GrowSP [91] to assign the same value for  $M^t$  across all 3D scenes, except for  $M^0$ .



### 3.3. Top-down Semantic Pseudo-label Generation

Having the full set of superpoints of all training scene point clouds, this module is designed to group all superpoints into semantic pseudo-labels, such that we can train a classification network for predicting per-point semantics. To achieve this goal, a naïve solution is using K-means to group all superpoints into semantic primitives by comparing the superpoint feature similarity, which is adopted by GrowSP [91]. However, such a simple clustering strategy, fundamentally, can only group per-point local features originally distilled from 2D domain, lacking the ability to capture additional and possibly richer semantic priors beyond local features.

A complex 3D scene is often composed by many flat planes, curved surfaces, straight edges, and sharp corners, which are crucial to describe 3D semantics. Intuitively, the differences between such features can be well-described in the frequency domain once 3D points are treated as signals. As illustrated in 2D domain in Figure 3, after an image is converted to frequency domain by 2D FFT, a low frequency component tends to indicate the general image background shape, whereas a higher frequency component likely represents shapes of minor objects or details.



Figure 3. An example of high and low frequency features in 2D.

With this insight, we aim to group superpoints in frequency domain which tends to capture semantic priors from a top-down perspective. Since 3D point clouds are irregular and orderless, directly applying 3D FFT is challenging and extremely computationally heavy [24]. In this regard, we turn to convert 3D point clouds into a global graph, and then apply Graph Fourier Transform (GFT) [62]. As also described in the rightmost block of Figure 2, this module involves the following three key steps.

#### 1) Constructing a Global Superpoint Graph

At the very beginning, the whole dataset has  $H$  point clouds and each point cloud has  $M^0$  superpoints, resulting in a total number of  $H * M^0$  superpoints, denoted as  $S = H * M^0$ . All superpoints have their own features, denoted as  $\tilde{\mathbf{F}} \in \mathbb{R}^{S \times 384}$ . Then, we build a global superpoint graph by treating each superpoint as a node, and the edge weight  $\mathbf{a}_{ij}$  between any  $i^{th}$  and  $j^{th}$  nodes is defined as follows:

$$\mathbf{a}_{ij} = \exp\left(-\|\tilde{\mathbf{f}}^i - \tilde{\mathbf{f}}^j\|_2\right) \quad (5)$$

where  $\tilde{\mathbf{f}}^i$  and  $\tilde{\mathbf{f}}^j$  are the  $i^{th}$  and  $j^{th}$  superpoint/node features extracted from  $\tilde{\mathbf{F}}$  respectively. This gives us a global graph  $G$  with  $S$  nodes and an adjacency matrix  $A \in \mathbb{R}^{S \times S}$  composed by all pairs of  $\mathbf{a}_{ij}$ .

For the global graph  $G$ , we compute its normalized Laplacian matrix  $L$  as follows:

$$L = D^{-1/2} \cdot (D - A) \cdot D^{-1/2}, \quad L \in \mathbb{R}^{S \times S} \quad (6)$$

where  $D$  is the diagonal matrix whose entries are the row-wise sum of the adjacency matrix  $A$ . Following GFT [62], the normalized Laplacian matrix  $L$  is decomposed into eigenvalues  $\Lambda$  and eigenvectors  $U$  as follows:

$$\begin{aligned} L &= U \cdot \Lambda \cdot U^T, \quad \Lambda, U \in \mathbb{R}^{S \times S} \\ U &= [\mathbf{u}^1 \cdots \mathbf{u}^s \cdots \mathbf{u}^S], \quad \mathbf{u}^s \in \mathbb{R}^{S \times 1} \end{aligned} \quad (7)$$

where each eigenvector in  $U$  represents a basis function or a specific frequency component, which can be naturally regarded as a specific *global pattern* jointly defined by all  $S$  superpoints. Clearly, the total  $S$  global patterns, *i.e.*, the  $S$  eigenvectors in  $U$ , encompass rich semantic priors.

#### 2) Grouping Global Patterns

Given the total  $S$  global patterns (eigenvectors), not all of them are uniquely meaningful in terms of 3D semantics. For example, for the same class *wall* superpoints, there could be multiple global patterns decomposed, where one pattern represents *wall* along  $x$ -axis and another pattern  $y$ -axis. Basically, these global patterns are not discriminative enough in semantics. To this end, we aim to group these patterns.

**First**, we transform all superpoint features  $\tilde{\mathbf{F}}$  to frequency domain via the total global patterns as follows:

$$\begin{aligned} \tilde{\mathbf{F}}_{freq} &= U^T \cdot \tilde{\mathbf{F}}, \quad \tilde{\mathbf{F}}_{freq} \in \mathbb{R}^{S \times 384} \\ \tilde{\mathbf{F}}_{freq} &= [\mathbf{f}_{freq}^1 \cdots \mathbf{f}_{freq}^s \cdots \mathbf{f}_{freq}^S]^T, \quad \mathbf{f}_{freq}^s \in \mathbb{R}^{1 \times 384} \end{aligned} \quad (8)$$

Mathematically, the  $s^{th}$  row vector  $\mathbf{f}_{freq}^s$  represents the frequency domain features projected from all superpoints' spatial features  $\tilde{\mathbf{F}}$ , corresponding to the  $s^{th}$  global pattern  $\mathbf{u}^s$ .

**Second**, we directly group all frequency domain vectors  $\{\mathbf{f}_{freq}^1 \cdots \mathbf{f}_{freq}^s \cdots \mathbf{f}_{freq}^S\}$  into  $S'$  clusters using K-means. Then, all the corresponding  $S$  global patterns  $\{\mathbf{u}^1 \cdots \mathbf{u}^s \cdots \mathbf{u}^S\}$  are assigned to the newly obtained  $S'$  clusters.

**Third**, for each of the new cluster, we merge its assigned global patterns by averaging them out to get a new cluster pattern, *i.e.*, a new global pattern as follows:

$$\mathbf{v}^{s'} = \frac{1}{W} \sum_{w=1}^W \mathbf{u}^w, \quad \mathbf{v}^{s'} \in \mathbb{R}^{S \times 1} \quad (9)$$

where  $W$  is the total number of global patterns within the  $s'$ -th cluster. Overall, the original  $S$  global patterns are grouped into  $S'$  new patterns:

$$\{\mathbf{v}^1 \cdots \mathbf{v}^{s'} \cdots \mathbf{v}^{S'}\} \xleftarrow{\text{K-means on } \tilde{\mathbf{F}}_{freq}} \{\mathbf{u}^1 \cdots \mathbf{u}^s \cdots \mathbf{u}^S\} \quad (10)$$

Our newly grouped global patterns, denoted as  $V = [\mathbf{v}^1 \cdots \mathbf{v}^{s'} \cdots \mathbf{v}^{S'}]$ , tend to have more meaningful semantic priors, fundamentally because the original patterns, which exhibit similar features in frequency domain, have been properly grouped in above steps.



### 3) Generating Semantic Pseudo-labels

Recall that, from the total  $S$  superpoints of the whole dataset, we firstly obtain its original  $S$  global patterns  $U = [u^1 \dots u^s \dots u^S]$ , and then group them into  $S'$  new global patterns  $V = [v^1 \dots v^{s'} \dots v^{S'}]$ , ( $V \in \mathbb{R}^{S \times S'}$ ). Regarding the new patterns  $V$ , its  $s^{th}$  row vector actually represents how the corresponding  $s^{th}$  superpoint contributes to the total  $S'$  new global patterns which encompass semantic priors. In other words, for a specific  $s^{th}$  superpoint  $\tilde{p}^s$ , the  $s^{th}$  row vector of  $V$ , denoted as  $\tilde{v}^s \in \mathbb{R}^{1 \times S'}$ , can be just regarded as a set of new features from the perspective of new global patterns in frequency domain.

With this insight, we directly group the total  $S$  superpoints into  $C$  semantic categories by applying K-means on the row vectors of  $V$ , thus generating semantic pseudo-labels for all superpoints as follows:

$$C \text{ classes} \xleftarrow{\text{K-means on } V} \{\tilde{p}^1 \dots \tilde{p}^s \dots \tilde{p}^S\} \quad (11)$$

### 3.4. Training / Testing

Given a dataset of point clouds and their associated images together with a self-supervised pretrained DINO/v2, the following Algorithm 1 summarizes how to link all our components to train a SparseConv model for predicting per-point semantics without needing human labels.

#### Algorithm 1 Local-global grouping of superpoints for training.

**Input:** Point clouds  $\{P^1 \dots P^h \dots P^H\}$ , images and DINO/v2;  
**Output:** Per-point semantic predictions belonging to  $C$  categories;  
**Init:** Obtain per-point 3D features via 2D distillation (Sec 3.1);  
 • Stage 1: Obtain initial superpoints (Step 1 of Sec 3.2), and group them into  $C$  (pseudo) classes (Sec 3.3);  
 • Stage 2: Assign pseudo labels to all single 3D points, and train a SparseConv model for  $E$  epochs using the standard cross-entropy loss;  
 • Stage 3: Use the new per-point features from trained SparseConv to grow the sizes of superpoints (Steps 2/3 of Sec 3.2);  
 • Stage 4: Group larger superpoints into  $C$  (pseudo) classes (Sec 3.3);  
 • Repeat the above Stages 2/3/4 for  $R$  rounds;  
**Return:** A well-trained SparseConv model to group per 3D point into  $C$  classes; Note that,  $C$  can be freely chosen in training/test. Our training loss exactly follows GrowSP [91].

After the network is well-trained, our evaluation setting exactly follows GrowSP to infer per-point semantics on test split, without needing to construct any superpoints. All implementation details and hyperparameters are in Appendices D to F.

## 4. Experiments

**Datasets:** We evaluate our method on two large-scale real-world indoor datasets: **1) ScanNet** [13] consisting of 1201 / 312 / 100 scenes for training, validation and online test respectively, **2) S3DIS** [2] including six large areas of indoor scenes, and a challenging outdoor dataset: **3) nuScenes** [3] encompassing LiDAR scans of outdoor autonomous driving scenes. We choose the latest self-supervised DINOv2 [46] as the pretrained model to distill features.

**Baselines:** We select the following baselines: **1) GrowSP** [91]: this is a pioneering work in unsupervised 3D semantic segmentation, but differs from us in two folds. First, it does not incorporate meaningful semantic priors for initial superpoints, but we leverage the self-supervised DINOv2 as a free lunch. Second, we introduce a new global grouping of superpoints in frequency domain to generate high-quality semantic pseudo-labels. **2) PointDC** [8], it utilizes a 2D pretrained model STEGO [20] based on DINO [5] for distilling features. For a fair comparison, we implement a DINOv2 version of PointDC, named as **3) PointDC-DINOv2**. **4) IIC** [27]. It is adapted from an existing unsupervised 2D method and modified to use the same backbone as ours. **5) PiCIE** [10]. It is also adapted from 2D domain with the same backbone as ours. **6) K-means** which is applied to cluster per-point  $xyzrgb$ .

**Metrics:** The standard metrics mean Intersection-over-Union (**mIoU**), Overall Accuracy (**OA**), and mean Accuracy (**mAcc**) across all classes are reported.

### 4.1. Evaluation on ScanNet

In ScanNet dataset, each point belongs to one of 20 object categories or undefined background. Exactly following GrowSP [91] and PointDC [8] in testing, we also use Hungarian matching to reorder the predicted labels for calculating scores, reporting results on both the offline validation and the online hidden test sets. The number of global patterns  $S'$  is set as 50, and the superpoint growing hyperparameters  $M^1$  and  $M^T$  are set as 80 and 40 for this dataset, and the number of rounds  $T$  as 5. Following GrowSP in training, all raw points are fed into the network and undefined points are excluded for loss computation.

**Results & Analysis:** As shown in Tables 1&2, our method clearly outperforms all unsupervised baselines by large margins on both val and test sets. PointDC-DINOv2 achieves higher scores than PointDC, but is much weaker than our LogoSP. This means that our bottom-up and top-down grouping of superpoints can indeed extract meaningful 3D semantics. As shown in Figure 4, we can see that existing baselines tend to group points into major categories, often overlooking minor classes such as *toilet*, whereas our method can effectively identify minor classes primarily because their features in frequency domain can be well captured by our method. More results are in Appendix D.

Table 1. Quantitative results on the **validation split** of ScanNet dataset [13]. All 20 categories are evaluated.

		OA(%)	mAcc(%)	mIoU(%)
Unsupervised	K-means	10.1	10.0	3.4
	IIC [27]	27.7	6.1	2.9
	PiCIE [10]	20.4	16.5	7.6
	GrowSP [91]	57.3	44.2	25.4
	PointDC [8]	63.7	-	25.7
	PointDC-DINOv2 [8]	64.7	45.0	29.6
	<b>LogoSP (Ours)</b>	<b>64.7</b>	<b>50.8</b>	<b>35.8</b>

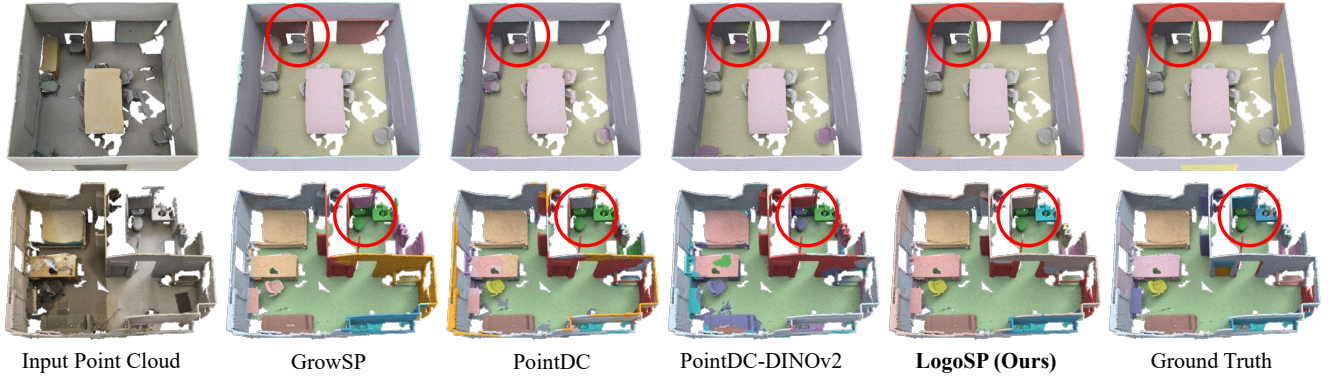


Figure 4. Qualitative results on ScanNet dataset (the first row) and S3DIS dataset (the second row). Red circles highlight the differences.

Table 2. Quantitative results on the **online hidden split** of ScanNet dataset [13]. All 20 categories are evaluated.

		mIoU(%)
Supervised	PointNet++ [55]	33.9
	PointCNN [36]	45.8
	SparseConv [16]	72.5
Unsupervised	GrowSP [91]	26.9
	PointDC [8]	22.9
	<b>LogoSP (Ours)</b>	<b>32.7</b>

## 4.2. Evaluation on S3DIS

S3DIS comprises 6 large areas with 271 rooms, where all points belong to 13 categories. In training, we follow GrowSP to exclude *clutter* points from loss computation and evaluation, as this category exhibits diverse geometric patterns across scenes without consistent semantics. We conduct experiments using standard 6-fold cross validation, training on 5 areas and evaluating on the remaining one. All hyperparameters are the same as used on ScanNet dataset.

**Results & Analysis:** As shown in Tables 3&4, our method outperforms all baselines on nearly all metrics. PointDC-DINOv2 and our method utilize DINOv2 features, but our method significantly surpasses it by 6% on Area-5 and 5% on the 6-fold setting on the important mIoU scores. Note that, due to the extremely sparse RGB images collected in this dataset, many 3D points do not correspond to 2D pixels and the distilled 3D features tend to be less discriminative, resulting in our method being just 2% higher than GrowSP on mIoU. Figure 4 compares qualitative results and more results are in Appendix E.

## 4.3. Evaluation on nuScenes

We also evaluate our method on a challenging outdoor dataset to demonstrate its generality. The nuScenes dataset contains 16 annotated categories for autonomous driving scenarios, including 28,130 LiDAR scenes aligned with RGB images for training and 6018 scenes for validation.

**Results & Analysis:** As shown in Table 5, our method achieves very encouraging results, outperforming all baselines. Notably, our method successfully identifies minor

Table 3. Quantitative results of our method and baselines on the Area-5 of S3DIS dataset [2]. Only 12 classes are evaluated.

		OA(%)	mAcc(%)	mIoU(%)
Supervised	PointNet [54]	77.5	59.1	44.6
	PointNet++ [55]	77.5	62.6	50.1
	SparseConv [16]	88.4	69.2	60.8
Unsupervised	K-means	21.4	21.2	8.7
	IIC [27]	28.5	12.5	6.4
	PiCIE [10]	61.6	25.8	17.9
	GrowSP [91]	78.4	57.2	44.5
	PointDC [8]	54.1	-	22.6
	PointDC-DINOv2 [8]	75.7	48.7	40.2
	<b>LogoSP (Ours)</b>	<b>82.8</b>	<b>55.9</b>	<b>46.5</b>

Table 4. Quantitative results of 6-fold cross validation on S3DIS dataset [2]. Only 12 classes excluding *clutter* are evaluated.

		OA(%)	mAcc(%)	mIoU(%)
Supervised	PointNet [54]	75.9	67.1	49.4
	PointNet++ [55]	77.1	74.1	55.1
	SparseConv [16]	89.4	78.1	69.2
Unsupervised	K-means	20.0	21.5	8.8
	IIC [27]	32.8	14.7	8.5
	PiCIE [10]	46.4	28.1	17.8
	GrowSP [91]	76.0	<b>59.4</b>	44.6
	PointDC [8]	55.7	37.7	26.0
	PointDC-DINOv2 [8]	74.4	51.5	41.3
	<b>LogoSP (Ours)</b>	<b>79.2</b>	58.0	<b>46.3</b>

categories such as *person* and *truck*, which are missed by all unsupervised baselines. Figure 5 shows qualitative results. More results are presented in Appendix F.

Table 5. Quantitative results on the **validation split** of nuScenes dataset [13]. All 16 categories are evaluated.

		OA(%)	mAcc(%)	mIoU(%)
Supervised	MinkUNet [12]	-	-	73.3
	Cylinder3D [95]	-	-	76.1
	SPVNAS [68]	-	-	77.4
Unsupervised	GrowSP [91]	39.2	17.5	10.2
	PointDC [8]	<b>56.8</b>	<b>29.4</b>	17.7
	PointDC-DINOv2 [8]	51.8	28.6	18.2
	<b>LogoSP (Ours)</b>	54.8	29.2	<b>20.1</b>

## 4.4. Generalization to Unseen Datasets

To verify that the learned semantic features are generic, we further conduct cross-dataset evaluations as follows:

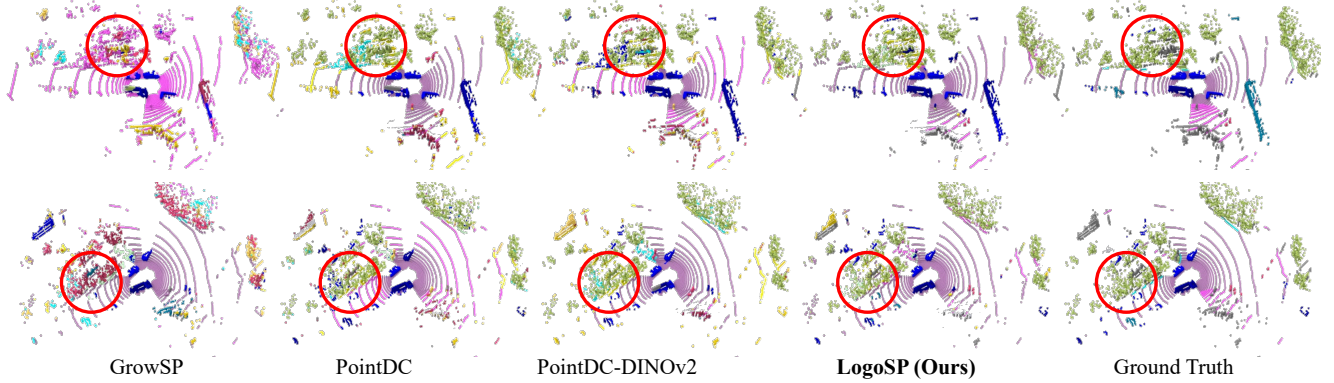


Figure 5. Qualitative results on the nuScenes dataset. Red circles highlight the differences.

1) **ScanNet to S3DIS**: We directly use the well-trained model on ScanNet in Section 4.1 to extract superpoint features from the ScanNet training set and cluster them into 12 centroids via K-means. These centroids serve as a classifier for the test areas of S3DIS.

2) **S3DIS to ScanNet**: Similarly, we use the well-trained model on S3DIS dataset in Section 4.2 to obtain 20 centroids from S3DIS training area features, and then evaluate them on the ScanNet validation set.

**Results & Analysis**: Table 6 shows results of generalization from ScanNet to S3DIS. We can see that our model trained on the ScanNet dataset significantly outperforms all baselines. Our mIoU scores are over 10% higher than all methods, primarily because ScanNet contains richer geometry patterns and semantic elements, and our model effectively retains these semantics by grouping global features in the frequency domain. In Table 7, all methods achieve rather low scores, though our LogoSP is still the best. The reason is that S3DIS dataset has limited 3D data (just 271 rooms) and sparse 2D images, making the learned semantic priors not generic enough overall.

Table 6. Generalization ability from ScanNet [13] to the unseen 6 areas of S3DIS [2]. The mIoU scores of 12 categories are reported.

test on $\rightarrow$	Area-1	Area-2	Area-3	Area-4	Area-5	Area-6	mean
IIC [27]	3.7	3.8	3.8	4.0	3.8	3.7	3.8
PiCIE [10]	13.5	12.7	13.4	12.8	11.3	13.1	12.8
GrowSP [91]	24.2	21.9	26.1	25.0	23.7	27.9	24.8
PointDC [8]	23.6	20.9	24.6	19.5	20.1	29.7	23.1
PointDC-DINOV2 [8]	33.8	29.6	33.8	31.7	32.2	36.9	33.0
<b>LogoSP (Ours)</b>	<b>43.8</b>	<b>37.5</b>	<b>47.0</b>	<b>40.7</b>	<b>44.9</b>	<b>47.9</b>	<b>43.6</b>

#### 4.5. Analysis of Global Patterns

By constructing a global superpoint graph  $G$ , we first obtain the total  $S$  global patterns (eigenvectors) in  $U$  via Equation 7. Then we group these global patterns into a new set of  $S'$  global patterns in  $V$  in Equation 10. These new global patterns tend to be much more semantically meaningful. To

Table 7. Generalization ability of models trained on different areas of S3DIS [2] to the unseen val split of ScanNet [13]. The mIoU scores of 20 categories are reported.

model trained on $\rightarrow$	Areas 2/3/4/5/6	Areas 1/3/4/5/6	Areas 1/2/4/5/6	Areas 1/2/3/5/6	Areas 1/2/3/4/6	Areas 1/2/3/4/5	mean
IIC [27]	3.5	3.4	3.7	3.5	3.5	3.6	3.5
PiCIE [10]	5.6	5.1	5.0	5.9	6.0	5.5	5.5
GrowSP [91]	16.9	<b>17.8</b>	16.4	16.1	<b>17.1</b>	15.3	16.6
PointDC [8]	10.3	10.1	10.4	8.4	10.0	9.9	9.9
PointDC-DINOV2 [8]	16.7	15.4	16.4	<b>17.6</b>	14.3	14.6	15.8
<b>LogoSP (Ours)</b>	<b>16.9</b>	16.9	<b>16.8</b>	16.8	16.7	<b>17.0</b>	<b>16.9</b>

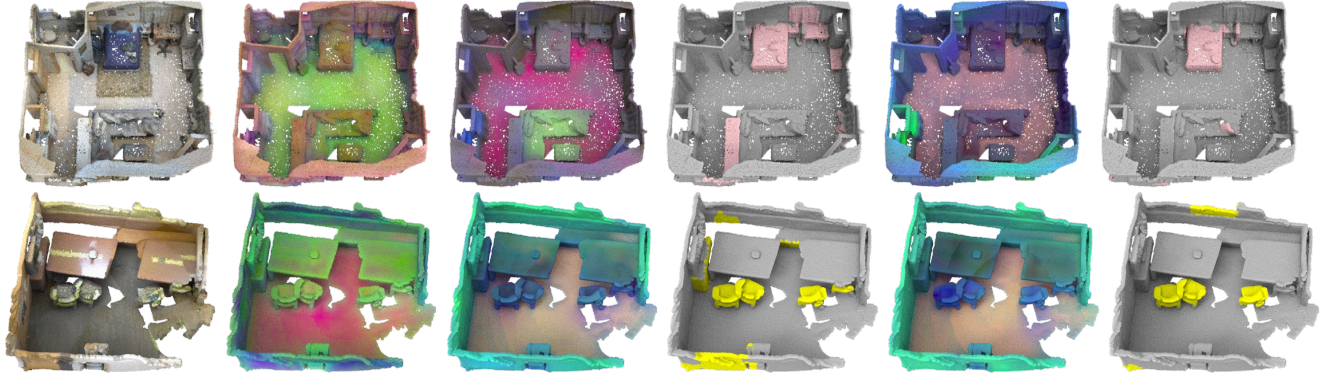
analyze what these new global patterns really learn, we conduct the following steps to visualize the patterns.

After training the backbone network on ScanNet dataset for a certain number of epochs, for each scene point cloud, we obtain its  $M^t$  superpoints, and we have a total number of  $M^t * 1201$  superpoints for the whole dataset. Then, we compute the set of  $S'$  global patterns  $V$  corresponding to the total superpoints. Third, we randomly pick up one of the  $S'$  global patterns: *i.e.*, a single  $M^t * 1201$  dimensional vector where each of the 1201 point clouds contributes an  $M^t$  dimensional sub-vector. After that, we randomly select one scene point cloud and its corresponding  $M^t$  dimensional sub-vector for analysis. At last, we visualize the relatively high values (salient global patterns in frequency domain) in the  $M^t$  dimensional sub-vector, by assigning a bright color to the corresponding superpoints. As shown in Figure 6, the 4<sup>th</sup> and 6<sup>th</sup> columns illustrate the salient global patterns at  $M^1$  and  $M^T$  respectively. For a comparison, we also visualize the per-point local features in 3D space, *i.e.*, a 384-dimensional vector, directly predicted from the backbone network. Clearly, we can see that, the global features in frequency domain tend to embed more and more meaningful semantics over the growth of superpoints during training.

#### 4.6. Ablation Study

To evaluate the effectiveness of each component of our method and the choices of hyperparameters, we conduct extensive ablation experiments on the ScanNet validation set.





Input Point Cloud    Distilled Features at  $M^0$     Point Features at  $M^1$     Global Pattern at  $M^1$     Point Features at  $M^T$     Global Pattern at  $M^T$   
Figure 6. Examples of a salient global pattern in each scene after grouping superpoints in frequency domain, and per-point local features.

**(1) Removing 2D-3D distillation:** Instead of training a model to distill 2D features to 3D, we simply copy DINOv2 pixel features to 3D points to grow superpoints and generate pseudo labels, and train a SparseConv from scratch.

**(2) ~ (3) Distilling from other self-supervised pre-trained models:** We also use DINO and STEGO models to distill 3D features in addition to the latest DINOv2.

**(4) Removing bottom-up superpoint growing:** We evaluate the effectiveness of superpoint growing, as it tends to cover larger areas to enrich the semantics.

**(5) ~ (8) Different choices of  $M^T$ :**  $M^T$  is the pre-defined number of superpoints at the end of growing. A smaller  $M^T$  indicates aggressive growing with larger superpoints in the end. We set  $M^T$  as 40 in main experiments.

**(9) ~ (11) Different choices of  $M^1$ :**  $M^1$  controls the number of superpoints at the beginning of growing. A greater  $M^1$  tends to be safer, while a smaller  $M^1$  may incur errors at early steps. We set  $M^1$  as 80 in main experiments.

**(12) Removing semantic pseudo-label generation:** We completely remove our third module top-down semantic pseudo-label generation. Instead, we use K-means to directly group per-point local features. Basically, this variant is GrowSP with distilled features from DINOv2.

**(13) ~ (17) Different choices of  $S'$ :** It controls how aggressive we group global patterns into new ones. Since global patterns in  $U$  may be redundant, clustering them could yield more discriminative representations. We set  $S'$  as 50 in main experiments.

**Analysis:** From Table 8, we can see that: 1) The distilled features are crucial to the pipeline as they provide high-quality semantic priors. 2) Superpoint growing is indeed helpful as well and it is relatively robust to its hyperparameters. 3) Without our new top-down grouping of global features in frequency domain, the performance clearly drops, demonstrating the effectiveness of our third component.

Table 8. The mIoU scores of all ablated networks on the validation set of ScanNet based on our full LogoSP.

	mIoU(%)
(1) Removing distillation	26.8
(2) Distilling DINO features	25.1
(3) Distilling STEGO features	25.8
(4) Removing superpoint growing	29.3
(6) $M^T = 50$	34.7
(7) $M^T = 40$	<b>35.8</b>
(8) $M^T = 30$	32.4
(9) $M^1 = 100$	35.7
(10) $M^1 = 80$	<b>35.8</b>
(11) $M^1 = 60$	32.1
(12) Removing semantic pseudo-label generation	31.4
(13) $S' = 30$	32.4
(14) $S' = 40$	32.6
(15) $S' = 50$	<b>35.8</b>
(16) $S' = 60$	35.6
(17) $S' = 70$	34.3
(18) The full framework (LogoSP)	<b>35.8</b>

## 5. Conclusion

Our proposed method learns per-point semantics from complex 3D scene point clouds without needing human labels in training. By leveraging the high-quality semantic priors distilled from self-supervised 2D features to 3D, we introduce a new global grouping strategy on superpoints to obtain highly accurate semantic pseudo-labels in the frequency domain. Extensive experiments on multiple benchmarks demonstrate the state-of-the-art performance of our method for 3D semantic segmentation. Nevertheless, our performance on the outdoor dataset is mixed, suggesting that DINOv2 features struggle to generalize to self-driving scenes. It would be interesting to extend our method for unsupervised semantic learning on sequential 3D point clouds.

**Acknowledgment:** This work was supported in part by National Natural Science Foundation of China under Grant 62271431, in part by Research Grants Council of Hong Kong under Grants 25207822 & 15225522.

## References

- [1] Rolf Adams and Leanne Bischof. Seeded region growing. *TPAMI*, 1994. [12](#)
- [2] Iro Armeni, Sasha Sax, Amir R. Zamir, and Silvio Savarese. Joint 2D-3D-Semantic Data for Indoor Scene Understanding. *arXiv:1702.01105*, 2017. [5](#), [6](#), [7](#)
- [3] Holger Caesar, Varun Bankiti, Alex H Lang, Sourabh Vora, Venice Erin Liong, and Qiang Xu. nuScenes: A multimodal dataset for autonomous driving. *CVPR*, 2020. [5](#)
- [4] Mathilde Caron, Piotr Bojanowski, Armand Joulin, and Matthijs Douze. Deep Clustering for Unsupervised Learning of Visual Features. *ECCV*, 2018. [2](#)
- [5] Mathilde Caron, Hugo Touvron, Ishan Misra, Hervé Jégou, Julien Mairal, Piotr Bojanowski, and Armand Joulin. Emerging Properties in Self-Supervised Vision Transformers. *ICCV*, 2021. [2](#), [3](#), [5](#)
- [6] Runnan Chen, Youquan Liu, Lingdong Kong, Xinge Zhu, Yuexin Ma, Yikang Li, Yuenan Hou, Yu Qiao, and Wenping Wang. CLIP2Scene: Towards Label-efficient 3D Scene Understanding by CLIP. *CVPR*, 2023. [2](#)
- [7] Ye Chen, Jinxian Liu, Bingbing Ni, Hang Wang, Jiancheng Yang, Ning Liu, Teng Li, Qi Tian, Huawei Hisilicon, Huawei Car Bu, and Huawei Cloud. Shape Self-Correction for Unsupervised Point Cloud Understanding. *ICCV*, 2021. [2](#)
- [8] Zisheng Chen, Hongbin Xu, Weitao Chen, Zhipeng Zhou, Haihong Xiao, Baigui Sun, Xuansong Xie, and Wenxiong Kang. Point DC: Unsupervised Semantic Segmentation of 3D Point Clouds via Cross-modal Distillation and Super-Voxel Clustering. *ICCV*, 2023. [1](#), [2](#), [3](#), [5](#), [6](#), [7](#), [14](#), [15](#), [16](#)
- [9] Julian Chibane, Francis Engelmann, Tuan Anh Tran, and Gerard Pons-Moll. Box2Mask: Weakly Supervised 3D Semantic Instance Segmentation Using Bounding Boxes. *ECCV*, 2022. [2](#)
- [10] Jang Hyun Cho, Utkarsh Mall, Kavita Bala, and Bharath Hariharan. PiCIE: Unsupervised Semantic Segmentation using Invariance and Equivariance in Clustering. *CVPR*, 2021. [2](#), [5](#), [6](#), [7](#), [14](#), [15](#), [16](#)
- [11] Christopher Choy, JunYoung Gwak, and Silvio Savarese. 4D Spatio-Temporal ConvNets: Minkowski Convolutional Neural Networks. *CVPR*, 2019. [2](#)
- [12] Christopher Choy, JunYoung Gwak, and Silvio Savarese. 4d spatio-temporal convnets: Minkowski convolutional neural networks. *CVPR*, 2019. [6](#)
- [13] Angela Dai, Angel X. Chang, Manolis Savva, Maciej Halber, Thomas Funkhouser, and Matthias Nießner. ScanNet: Richly-annotated 3D Reconstructions of Indoor Scenes. *CVPR*, 2017. [5](#), [6](#), [7](#)
- [14] Runyu Ding, Jihan Yang, Chuhui Xue, Wenqing Zhang, Song Bai, and Xiaojuan Qi. PLA: Language-Driven Open-Vocabulary 3D Scene Understanding. *CVPR*, 2023. [2](#)
- [15] Wouter Van Gansbeke, Simon Vandenhende, and Stamatios Georgoulis. Unsupervised Semantic Segmentation by Contrasting Object Mask Proposals. *ICCV*, 2021. [2](#)
- [16] Benjamin Graham, Martin Engelcke, and Laurens van der Maaten. 3D Semantic Segmentation with Submanifold Sparse Convolutional Networks. *CVPR*, 2018. [1](#), [2](#), [3](#), [6](#), [14](#), [15](#), [16](#)
- [17] Haoyu Guo, He Zhu, Sida Peng, Yuang Wang, Yujun Shen, Ruizhen Hu, and Xiaowei Zhou. SAM-guided Graph Cut for 3D Instance Segmentation. *ECCV*, 2024. [2](#)
- [18] Meng-Hao Guo, Jun-Xiong Cai, Zheng-Ning Liu, Tai-Jiang Mu, Ralph R. Martin, and Shi-Min Hu. PCT: Point Cloud Transformer. *Computational Visual Media*, 2021. [2](#)
- [19] Huy Ha and Shuran Song. Semantic Abstraction: Open-World 3D Scene Understanding from 2D Vision-Language Models. *CoRL*, 2022. [2](#)
- [20] Mark Hamilton, Zhoutong Zhang, Bharath Hariharan, Noah Snaveley, and William T. Freeman. Unsupervised Semantic Segmentation by Distilling Feature Correspondences. *ICLR*, 2022. [2](#), [5](#)
- [21] Ji Hou, Benjamin Graham, Matthias Nießner, and Saining Xie. Exploring Data-Efficient 3D Scene Understanding with Contrastive Scene Contexts. *CVPR*, 2021. [2](#)
- [22] Qingyong Hu, Bo Yang, Linhai Xie, Stefano Rosa, Yulan Guo, Zhihua Wang, Niki Trigoni, and Andrew Markham. RandLA-Net: Efficient Semantic Segmentation of Large-Scale Point Clouds. *CVPR*, 2020. [1](#), [2](#)
- [23] Qingyong Hu, Bo Yang, Linhai Xie, Stefano Rosa, Yulan Guo, Zhihua Wang, Niki Trigoni, and Andrew Markham. Learning Semantic Segmentation of Large-scale Point Clouds with Random Sampling. *TPAMI*, 2021. [2](#)
- [24] Qianjiang Hu, Daizong Liu, and Wei Hu. Exploring the devil in graph spectral domain for 3d point cloud attacks. *ECCV*, 2022. [4](#)
- [25] Qingyong Hu, Bo Yang, Guangchi Fang, Yulan Guo, Ales Leonardis, Niki Trigoni, and Andrew Markham. SQN: Weakly-Supervised Semantic Segmentation of Large-Scale 3D Point Clouds. *ECCV*, 2022. [1](#), [2](#)
- [26] Siyuan Huang, Yichen Xie, Song-Chun Zhu, and Yixin Zhu. Spatio-temporal Self-Supervised Representation Learning for 3D Point Clouds. *ICCV*, 2021. [2](#)
- [27] Xu Ji, Andrea Vedaldi, and Joao Henriques. Invariant information clustering for unsupervised image classification and segmentation. *ICCV*, 2019. [2](#), [5](#), [6](#), [7](#), [14](#), [15](#), [16](#)
- [28] Chanyoung Kim, Woojung Han, Dayun Ju, and Seong Jae Hwang. EAGLE: Eigen Aggregation Learning for Object-Centric Unsupervised Semantic Segmentation. *CVPR*, 2024. [2](#)
- [29] Hyeonseong Kim, Sung-Hoon Yoon, Minseok Kim, and Kuk-Jin Yoon. On-the-fly Category Discovery for LiDAR Semantic Segmentation. *ECCV*, 2024. [2](#)
- [30] Alexander Kirillov, Eric Mintun, Nikhila Ravi, Hanzi Mao, Chloe Rolland, Laura Gustafson, Tete Xiao, Spencer Whitehead, Alexander C. Berg, Wan-Yen Lo, Piotr Dollár, and Ross Girshick. Segment Anything. *ICCV*, 2023. [1](#), [2](#)
- [31] Maxim Kolodiaznyi, Anna Vorontsova, Anton Konushin, and Danila Rukhovich. OneFormer3D: One Transformer for Unified Point Cloud Segmentation. *CVPR*, 2024. [2](#)
- [32] Abhijit Kundu, Xiaoqi Yin, Alireza Fathi, David Ross, Brian Brewington, Thomas Funkhouser, and Caroline Pantofaru. Virtual multi-view fusion for 3D semantic segmentation. *ECCV*, 2020. [2](#)

- [33] Loic Landrieu and Martin Simonovsky. Large-scale point cloud semantic segmentation with superpoint graphs. *CVPR*, 2018. 2
- [34] Huan Lei, Naveed Akhtar, and Ajmal Mian. Octree guided CNN with Spherical Kernels for 3D Point Clouds. *CVPR*, 2019. 2
- [35] Xiang Li, Jian Ding, Zhaoyang Chen, and Mohamed Elhoseiny. Uni3DL: A Unified Model for 3D Vision-Language Understanding. *ECCV*, 2024. 2
- [36] Yangan Li, Rui Bu, Mingchao Sun, Wei Wu, Xinhan Di, and Baoquan Chen. PointCNN: Convolution On X-Transformed Points. *NIPS*, 2018. 2, 6, 14
- [37] Jiaxu Liu, Zhengdi Yu, Toby P. Breckon, and Hubert P.H. Shum. U3DS3: Unsupervised 3D Semantic Scene Segmentation. *WACV*, 2024. 1
- [38] Kangcheng Liu, Yuzhi Zhao, Qiang Nie, Zhi Gao, and Ben M. Chen. Weakly Supervised 3D Scene Parsing with Region-Level Boundary Awareness and Instance Discrimination. *ECCV*, 2022. 2
- [39] Minghua Liu, Yin Zhou, Charles R Qi, Boqing Gong, Hao Su, and Dragomir Anguelov. LESS: Label-Efficient Semantic Segmentation for LiDAR Point Clouds. *ECCV*, 2022. 2
- [40] Youquan Liu, Lingdong Kong, Jun Cen, Runnan Chen, Wenwei Zhang, Liang Pan, Kai Chen, and Ziwei Liu. Segment Any Point Cloud Sequences by Distilling Vision Foundation Models. *NeurIPS*, 2023. 2
- [41] Zhijian Liu, Haotian Tang, Yujun Lin, and Song Han. Point-Voxel CNN for Efficient 3D Deep Learning. *NeurIPS*, 2019. 2
- [42] Zhengzhe Liu, Xiaojuan Qi, and Chi-Wing Fu. One Thing One Click: A Self-Training Approach for Weakly Supervised 3D Semantic Segmentation. *CVPR*, 2021. 2
- [43] Hsien-Yu Meng, Gao Lin, Yu-Kun Lai, and Dinesh Manocha. VV-Net: Voxel VAE Net with Group Convolutions for Point Cloud Segmentation. *ICCV*, 2019. 2
- [44] Andres Milioto, Ignacio Vizzo, Jens Behley, and Cyrill Stachniss. RangeNet++: Fast and Accurate LiDAR Semantic Segmentation. *IROS*, 2019. 2
- [45] Oona Oinonen, Lassi Ruoppa, Josef Taher, Matti Lehtomäki, Leena Matikainen, Kirsi Karila, Teemu Hakala, Antero Kukko, Harri Kaartinen, and Juha Hyypä. Unsupervised semantic segmentation of urban high-density multispectral point clouds. *arXiv:2410.18520*, 2024. 1
- [46] Maxime Oquab, Timothée Darcet, Théo Moutakanni, Huy V Vo, Marc Szafraniec, Vasil Khalidov, Pierre Fernandez, Daniel Haziza, Francisco Massa, Alaaeldin El-nouby, Mahmoud Assran, Nicolas Ballas, Wojciech Galuba, Russell Howes, Po-yao Huang, Shang-wen Li, Ishan Misra, Michael Rabbat, Vasu Sharma, Gabriel Synnaeve, Hu Xu, Hervé Jegou, and Julien Mairal. DINOv2: Learning Robust Visual Features without Supervision. *TMLR*, 2024. 2, 3, 5
- [47] Aljoša Ošep, Tim Meinhardt, Francesco Ferroni, Neehar Peri, Deva Ramanan, and Laura Leal-Taixé. Better Call SAL: Towards Learning to Segment Anything in Lidar. *ECCV*, 2024. 2
- [48] Yassine Ouali, Céline Hudelot, and Myriam Tami. Autoregressive Unsupervised Image Segmentation. *ECCV*, 2020. 2
- [49] Yatian Pang, Wenxiao Wang, Francis E. H. Tay, Wei Liu, Yonghong Tian, and Li Yuan. Masked Autoencoders for Point Cloud Self-supervised Learning. *ECCV*, 2022. 2
- [50] Jeremie Papon, Alexey Abramov, Markus Schoeler, and Florentin Worgotter. Voxel cloud connectivity segmentation-supervoxels for point clouds. *CVPR*, 2013. 12
- [51] Bohao Peng, Xiaoyang Wu, Li Jiang, Yukang Chen, Hengshuang Zhao, Zhuotao Tian, and Jiaya Jia. OA-CNNs: Omni-Adaptive Sparse CNNs for 3D Semantic Segmentation. *CVPR*, 2024. 2
- [52] Songyou Peng, Kyle Genova, Chiyu "Max" Jiang, Andrea Tagliasacchi, Marc Pollefeys, and Thomas Funkhouser. OpenScene: 3D Scene Understanding with Open Vocabularies. *CVPR*, 2023. 2, 3
- [53] Xidong Peng, Runnan Chen, Feng Qiao, Lingdong Kong, Youquan Liu, Yujing Sun, Tai Wang, Xinge Zhu, and Yuexin Ma. Learning to Adapt SAM for Segmenting Cross-Domain Point Clouds. *ECCV*, 2024. 2
- [54] Charles R. Qi, Hao Su, Kaichun Mo, and Leonidas J. Guibas. PointNet: Deep Learning on Point Sets for 3D Classification and Segmentation. *CVPR*, 2017. 1, 2, 6, 15, 16
- [55] Charles R. Qi, Li Yi, Hao Su, and Leonidas J. Guibas. PointNet++: Deep Hierarchical Feature Learning on Point Sets in a Metric Space. *NIPS*, 2017. 2, 6, 14, 15, 16
- [56] Alec Radford, Jong Wook Kim, Chris Hallacy, Aditya Ramesh, Gabriel Goh, Sandhini Agarwal, Girish Sastry, Amanda Askell, Pamela Mishkin, Jack Clark, Gretchen Krueger, and Ilya Sutskever. Learning Transferable Visual Models From Natural Language Supervision. *ICML*, 2021. 1, 2
- [57] Yongming Rao, Jiwen Lu, and Jie Zhou. Global-Local Bidirectional Reasoning for Unsupervised Representation Learning of 3D Point Clouds. *CVPR*, 2020. 2
- [58] Nikhila Ravi, Valentin Gabeur, Yuan-Ting Hu, Ronghang Hu, Chaitanya Ryali, Tengyu Ma, Haitham Khedr, Roman Rädle, Chloe Rolland, Laura Gustafson, Eric Mintun, Junting Pan, Kalyan Vasudev Alwala, Nicolas Carion, Chao-Yuan Wu, Ross Girshick, Piotr Dollár, and Christoph Feichtenhofer. SAM 2: Segment Anything in Images and Videos. *arXiv:2408.00714*, 2024. 2
- [59] Damien Robert, Hugo Raguét, and Loic Landrieu. Efficient 3d semantic segmentation with superpoint transformer. *ICCV*, 2023. 2
- [60] David Rozenberszki, Or Litany, and Angela Dai. Language-Grounded Indoor 3D Semantic Segmentation in the Wild. *ECCV*, 2022. 2
- [61] Lassi Ruoppa, Oona Oinonen, Josef Taher, Matti Lehtomäki, Narges Takhtkeshha, Antero Kukko, Harri Kaartinen, and Juha Hyypä. Unsupervised deep learning for semantic segmentation of multispectral LiDAR forest point clouds. *arXiv:2502.06227*, 2025. 1
- [62] Aliaksei Sandryhaila and José MF Moura. Discrete signal processing on graphs: Graph fourier transform. *ICASSP*, 2013. 4
- [63] Jonathan Sauder and Bjarne Sievers. Self-Supervised Deep Learning on Point Clouds by Reconstructing Space. *NeurIPS*, 2019. 2



- [64] Jonas Schult, Francis Engelmann, Alexander Hermans, Or Litany, Siyu Tang, and Bastian Leibe. Mask3D: Mask Transformer for 3D Semantic Instance Segmentation. *ICRA*, 2023. 2
- [65] Hyun Seok Seong, WonJun Moon, SuBeen Lee, and Jae-Pil Heo. Progressive Proxy Anchor Propagation for Unsupervised Semantic Segmentation. *ECCV*, 2024. 2
- [66] Hanyu Shi, Jiacheng Wei, Ruibo Li, Fayao Liu, and Guosheng Lin. Weakly Supervised Segmentation on Outdoor 4D point clouds with Temporal Matching and Spatial Graph Propagation. *CVPR*, 2022. 2
- [67] Weiwei Sun, Andrea Tagliasacchi, Boyang Deng, Sara Sabour, Soroosh Yazdani, Geoffrey Hinton, and Kwang Moo Yi. Canonical Capsules: Unsupervised Capsules in Canonical Pose. *NeurIPS*, 2021. 2
- [68] Haotian Tang, Zhijian Liu, Shengyu Zhao, Yujun Lin, Ji Lin, Hanrui Wang, and Song Han. Searching efficient 3d architectures with sparse point-voxel convolution. *ECCV*, 2020. 6, 16
- [69] Anh Thai, Weiyao Wang, Hao Tang, Stefan Stojanov, Matt Feiszli, and James M. Rehg. 3x2: 3D Object Part Segmentation by 2D Semantic Correspondences. *ECCV*, 2024. 2
- [70] Hugues Thomas, Charles R. Qi, Jean-Emmanuel Deschaud, Beatriz Marcotegui, François Goulette, and Leonidas J. Guibas. KPConv: Flexible and Deformable Convolution for Point Clouds. *ICCV*, 2019. 2
- [71] Hugues Thomas, Yao-hung Hubert Tsai, Timothy D Barfoot, and Jian Zhang. KPConvX: Modernizing Kernel Point Convolution with Kernel Attention. *CVPR*, 2024. 2
- [72] Ardian Umam, Cheng-Kun Yang, Jen-Hui Chuang, and Yen-Yu Lin. Unsupervised Point Cloud Co-part Segmentation via Co-attended Superpoint Generation and Aggregation. *TMM*, 2024. 1
- [73] Ozan Unal, Dengxin Dai, and Luc Van Gool. Scribble-Supervised LiDAR Semantic Segmentation. *CVPR*, 2022. 2
- [74] Hanchen Wang, Qi Liu, Xiangyu Yue, Joan Lasenby, and Matthew J. Kusner. Unsupervised Point Cloud Pre-Training via Occlusion Completion. *ICCV*, 2021. 2
- [75] Yue Wang, Yongbin Sun, Ziwei Liu, Sanjay E. Sarma, Michael M. Bronstein, and Justin M. Solomon. Dynamic Graph CNN for Learning on Point Clouds. *TOG*, 38, 2019. 2, 14
- [76] Jiacheng Wei, Guosheng Lin, Kim-Hui Yap, Tzu-Yi Hung, and Lihua Xie. Multi-Path Region Mining For Weakly Supervised 3D Semantic Segmentation on Point Clouds. *CVPR*, 2020. 2
- [77] Bichen Wu, Alvin Wan, Xiangyu Yue, and Kurt Keutzer. SqueezeSeg: Convolutional Neural Nets with Recurrent CRF for Real-Time Road-Object Segmentation from 3D LiDAR Point Cloud. *ICRA*, 2018. 1, 2
- [78] Wenxuan Wu, Zhongang Qi, and Li Fuxin. PointConv: Deep Convolutional Networks on 3D Point Clouds. *CVPR*, 2019. 2
- [79] Zhonghua Wu, Yicheng Wu, Guosheng Lin, Jianfei Cai, and Chen Qian. Dual Adaptive Transformations for Weakly Supervised Point Cloud Segmentation. *ECCV*, 2022. 2
- [80] Zihao Xiao, Longlong Jing, Shangxuan Wu, Alex Zihao Zhu, Jingwei Ji, Chiyu Max Jiang, Wei-chih Hung, Thomas Funkhouser, and Weicheng Kuo. 3D Open-Vocabulary Panoptic Segmentation with 2D-3D Vision-Language Distillation. *ECCV*, 2024. 2
- [81] Saining Xie, Jiatao Gu, Demi Guo, Charles R Qi, Leonidas Guibas, and Or Litany. PointContrast: Unsupervised Pre-training for 3D Point Cloud Understanding. *ECCV*, 2020. 2
- [82] Jinfeng Xu, Siyuan Yang, Xianzhi Li, Yuan Tang, Yixue Hao, Long Hu, and Min Chen. PDF: A Probability-Driven Framework for Open World 3D Point Cloud Semantic Segmentation. *CVPR*, 2024. 2
- [83] Ruijie Xu, Chuyu Zhang, Hui Ren, and Xuming He. Dual-level Adaptive Self-Labeling for Novel Class Discovery in Point Cloud Segmentation. *ECCV*, 2024.
- [84] Jihan Yang, Runyu Ding, Zhe Wang, and Xiaojuan Qi. RegionPLC: Regional Point-Language Contrastive Learning for Open-World 3D Scene Understanding. *CVPR*, 2024.
- [85] Yingda Yin, Yuzheng Liu, Yang Xiao, Daniel Cohen-Or, Jingwei Huang, and Baoquan Chen. SAI3D: Segment Any Instance in 3D Scenes. *CVPR*, 2024. 2
- [86] Zhaoyuan Yin, Pichao Wang, Fan Wang, Xianzhe Xu, Hanling Zhang, Hao Li, and Rong Jin. TransFGU: A Top-down Approach to Fine-Grained Unsupervised Semantic Segmentation. *ECCV*, 2022. 2
- [87] Andrii Zadaianchuk, Matthaeus Kleindessner, Yi Zhu, Francesco Locatello, and Thomas Brox. Unsupervised Semantic Segmentation with Self-supervised Object-Centric Representations. *ICLR*, 2023. 2
- [88] Yachao Zhang, Yanyun Qu, Yuan Xie, Zonghao Li, Shanshan Zheng, and Cuihua Li. Perturbed Self-Distillation: Weakly Supervised Large-Scale Point Cloud Semantic Segmentation. *ICCV*, 2021. 2
- [89] Zaiwei Zhang, Rohit Girdhar, Armand Joulin, and Ishan Misra. Self-Supervised Pretraining of 3D Features on any Point-Cloud. *ICCV*, 2021. 2
- [90] Zaiwei Zhang, Min Bai, and Erran Li. Self-Supervised Pre-training for Large-Scale Point Clouds. *NeurIPS*, 2022. 2
- [91] Zihui Zhang, Bo Yang, Bing Wang, and Bo Li. GrowSP: Unsupervised Semantic Segmentation of 3D Point Clouds. *CVPR*, 2023. 1, 2, 3, 4, 5, 6, 7, 12, 13, 14, 15, 16
- [92] Zhaoxiang Zhang, Ankang Ji, Zhuan Xia, Limao Zhang, Yuelei Xu, and Qing Zhou. Unsupervised seepage segmentation pipeline based on point cloud projection with large vision model. *Tunnelling and Underground Space Technology*, 2025. 1
- [93] Hengshuang Zhao, Li Jiang, Jiaya Jia, Philip Torr, and Vladlen Koltun. Point Transformer. *ICCV*, 2021. 2
- [94] Chong Zhou, Chen Change Loy, and Bo Dai. Extract Free Dense Labels from CLIP. *ECCV*, 2022. 2
- [95] Xinge Zhu, Hui Zhou, Tai Wang, Fangzhou Hong, Yuexin Ma, Wei Li, Hongsheng Li, and Dahua Lin. Cylindrical and Asymmetrical 3D Convolution Networks for LiDAR Segmentation. *CVPR*, 2021. 2, 6, 16

## Appendix

### A. Initial Superpoint Generation

In this section, we describe the detailed steps to generate initial superpoints on three datasets. For the two indoor datasets ScanNet and S3DIS, we adhere to the steps outlined in GrowSP [91], utilizing Voxel Cloud Connectivity Segmentation (VCCS) [50] and Region Growing [1] while maintaining the same parameters used in GrowSP. Figure 7 illustrates examples of ScanNet and S3DIS datasets.

For the outdoor dataset nuScenes, we adapt from GrowSP by employing RANSAC and Euclidean Clustering to generate superpoints. Initially, RANSAC is applied to identify a large planar surface, designated as the ground. Subsequently, the remaining 3D points are partitioned into clusters using Euclidean Clustering. In RANSAC, points within 0.2 meters of the fitted plane are classified as plane points and aggregated into a single superpoint. For the remaining points, those with an Euclidean distance of less than 0.2 meters are grouped into a single superpoint. Qualitative examples are shown in Figure 7.

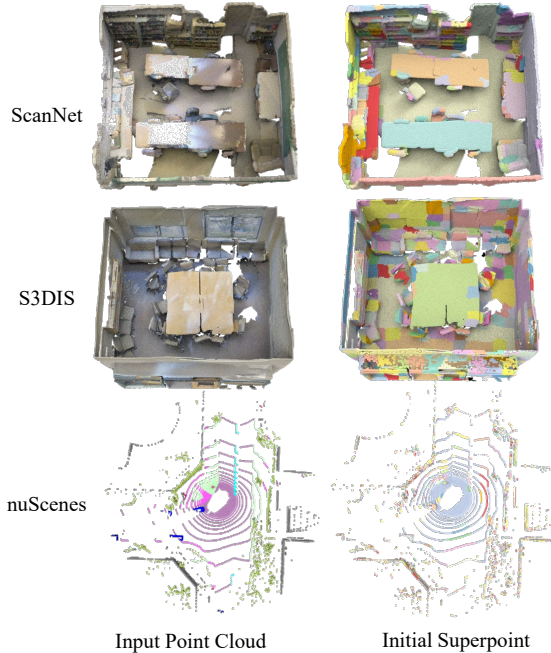


Figure 7. Examples of initial superpoints.

### B. Additional Ablation Study

We conduct additional ablation studies to examine the impact of the semantic category number, distillation process, and segmentation component.

**(1) K-means on distilled features:** The distilled point features appear to be aware of semantics, thus we apply K-

Table 9. The mIoU scores of all ablated networks on the validation set of ScanNet based on our full LogoSP.

	mIoU(%)
(1) K-means on distilled features	18.2
(2) GrowSP with distillation	27.4
(3) $C = 10$	32.8
(4) $C = 15$	33.7
<b>(5) <math>C = 20</math></b>	<b>35.8</b>
(6) $C = 30$	34.7
(7) $C = 50$	32.9
<b>(8) The full framework (LogoSP)</b>	<b>35.8</b>

means on the distilled point features of ScanNet val set to cluster into 20 classes.

**(2) GrowSP with distillation:** To demonstrate the effectiveness of our global grouping strategy, we apply the well-trained distillation model to GrowSP and complete its subsequent training.

**(3) ~ (7):** In our experiments,  $C$  is set as 20 for ScanNet, but it can be freely chosen in training. To verify it, we adopt different values:  $\{10, 15, 20, 30, 50\}$ .

**Analysis:** From Table 9, we can see that: 1) A simple K-means is not sufficient to discover semantics from the distilled features, so the top-down semantic pseudo-label generation is necessary. 2) GrowSP can be also benefited from the distillation, but the gap between 27.4 and 35.8 indicates our global patterns in the frequency domain is more aligned with semantics. 3)  $C$  can be flexible, though too large or too small is not preferred.

### C. Impacts of Initial Superpoint Purity

The initial superpoints are crucial in our LogoSP. If the initial superpoints extensively cover points from different categories, it can lead to a decline in segmentation performance. To measure this, we define the purity of superpoints as follows: we use ground truth semantic labels to assign a unique label to each superpoint through a voting process. Consequently, all points receive a label generated from this voting. We then compute the mIoU between these voting labels and the ground truth to assess the purity of initial superpoints.

The initial superpoints are constructed by VCCS and Region Growing, the smaller resolutions of VCCS yield purer superpoints, and the higher the mIoU against GT, the purer. As shown in Table 10, we obtain robust results even at rather low purity on ScanNet val.

Another interesting observation is the trend of purity over the growing process. From Table 11, when  $M^i$  is reduced to  $M^0 \rightarrow 80/70/60/50/40$ , the superpoint purity (mIoU) drops  $76.8 \rightarrow 74.6/73.8/72.6/71.4/69.4$  as expected.

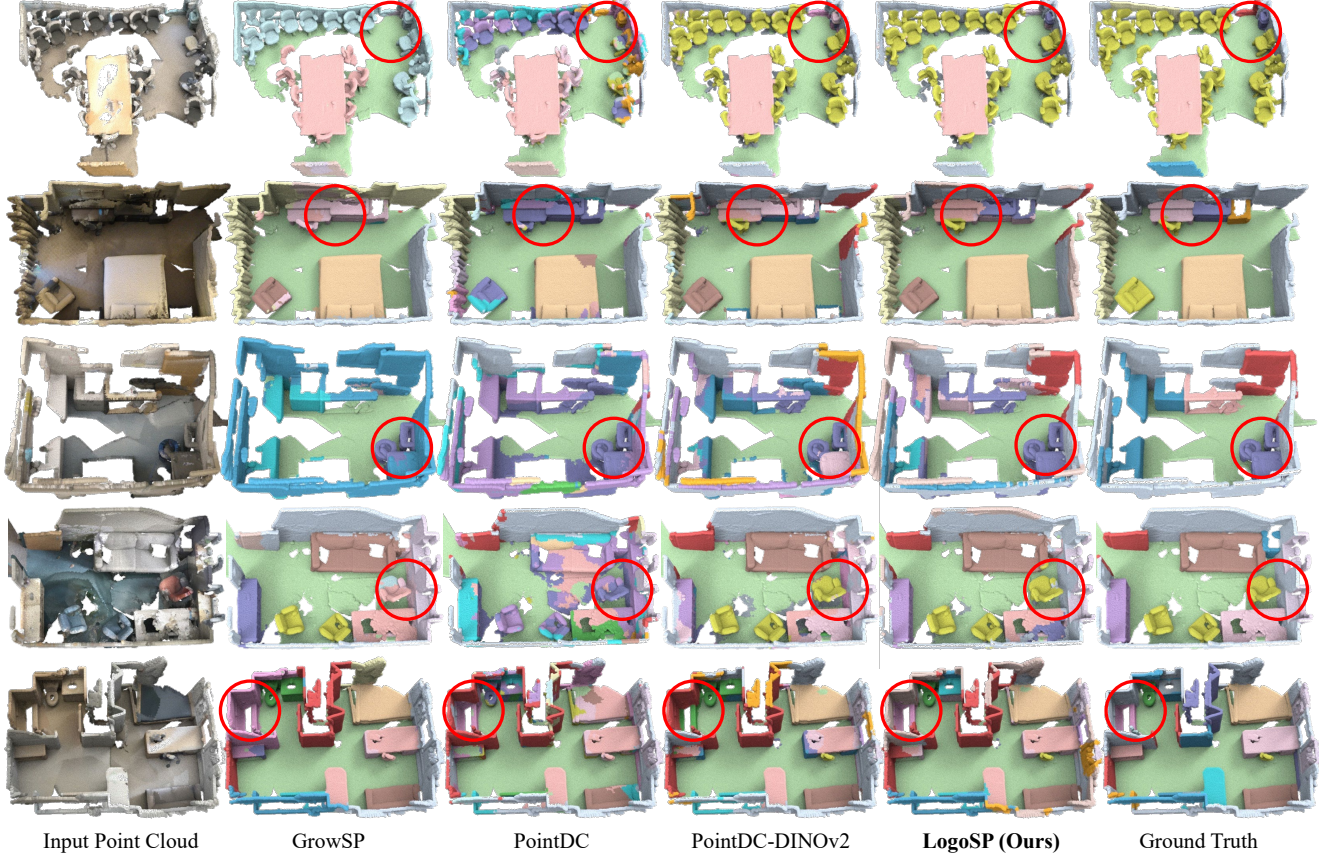


Figure 8. Qualitative results of our method and baselines on the validation set of ScanNet dataset.

Table 10. Impact of initial superpoint purity on ScanNet val.

resolution (m)	0.1	0.3	0.5	0.7	0.9
Initial superpoint purity (mIoU)	83.9	81.7	76.8	71.7	66.1
Segmentation results (mIoU)	34.7	35.9	35.8	34.8	31.3

Table 11. Trend of purity over growing.

Number of superpoints ( $M^i$ )	$M^0$	80	70	60	50	40
Superpoints purity (mIoU)	76.8	74.6	73.8	72.6	71.4	69.4

## D. Evaluation on ScanNet

When evaluating on the ScanNet dataset, we utilize SparseConv as our backbone which is the same as GrowSP[91]. A voxel size of 5cm is employed to convert point clouds into voxel grids for both distillation and segmentation tasks. For distillation, we select the ViT-S/14 version of DINOv2 as the 2D feature extractor for our method and the baseline PointDC-DINOv2. The distillation process is conducted over 200 epochs with a batch size of 8, a learning rate of  $1e-3$ , and the Adam optimizer. The Poly scheduler is used to progressively decrease the learning rate. For training our segmentation network, we employ cross-entropy as the loss

function, maintaining a batch size of 8 and a constant learning rate of  $1e-4$  with the Adam optimizer over 200 epochs. The superpoints growing parameters  $M^1$  and  $M^T$  are set as 80 and 40. The extraction of global patterns and generation of pseudo labels are conducted every 10 epochs.

The per-category results on both validation and hidden test sets are detailed in Tables 12&13. Our method significantly outperforms all unsupervised baselines, particularly on minor classes such as *books*, *curtain*, and *toilet*. Figure 8 provides further comparisons with baselines.

## E. Evaluation on S3DIS

Prior to training, we downsample input point clouds by applying grid sampling with a 0.01m grid size. Distillation and segmentation are then performed on the downsampled data. Same as ScanNet, we also choose ViT-S/14 of DINOv2 model in the configuration. For distillation, we choose the learning rate of  $1e-3$ , the Adam optimizer, and the Poly scheduler. When training the segmentation network, we employ a learning rate of  $1e-4$  over 200 epochs, with the parameter  $S'$  for grouping global patterns being 10.  $M^1$  and  $M^T$  are also set as 80 and 40 respectively.



Table 12. Per-category quantitative results on the validation split of ScanNet dataset.

	OA(%)	mAcc(%)	mIoU(%)	wall.	floor.	cab.	bed.	chair.	sofa.	table	door.	wind.	books.	pic.	counter.	desk.	curtain.	fridge.	shower.	toilet.	sink.	bathub.	otherf.
K-means	10.1	10.0	3.4	9.0	9.8	3.2	2.9	5.5	3.3	4.3	3.5	5.5	3.3	<b>2.6</b>	0.8	2.9	4.3	0.8	0.7	0.3	0.9	4.0	
IIC [27]	27.7	6.1	2.9	25.3	20.5	0.6	0.3	3.7	0.4	1.3	1.3	1.1	1.9	0.2	0.1	0.6	0.3	0.4	0	0	0	0.2	0.5
PICIE [10]	20.4	16.5	7.6	14.7	24.5	6.3	5.2	18.0	8.4	33.2	6.7	4.8	9.3	2.1	0.1	2.7	8.0	1.1	2.1	0	0	0.5	5.0
GrowSP [91]	57.3	44.2	25.4	40.7	89.8	<b>24.0</b>	47.2	45.5	43.0	39.4	14.1	20.0	53.5	0.1	5.4	13.3	8.4	<b>2.1</b>	<b>11.3</b>	20.6	<b>19.4</b>	0	9.8
PointDC [8]	62.4	38.8	26.0	<b>59.1</b>	<b>94.0</b>	22.0	43.2	30.4	35.9	38.3	14.3	37.4	44.4	1.2	2.4	2.3	<b>39.4</b>	2.0	0	38.6	0	2.2	12.7
PointDC-DINOv2 [8]	64.7	45.0	29.6	57.0	86.0	18.5	60.6	60.1	46.2	46.4	27.0	39.0	54.2	0.7	25.0	<b>18.1</b>	22.7	0.2	2.8	16.8	0	0	10.4
<b>LogoSP (Ours)</b>	<b>64.7</b>	<b>50.8</b>	<b>35.8</b>	46.3	86.6	20.7	<b>66.8</b>	<b>63.3</b>	<b>50.9</b>	<b>47.1</b>	<b>33.8</b>	<b>41.6</b>	<b>62.8</b>	1.0	<b>38.0</b>	10.5	28.6	0.5	0	<b>46.3</b>	0	<b>42.3</b>	<b>29.6</b>

Table 13. Per-category quantitative results on the hidden test split of ScanNet dataset.

		mIoU(%)	wall.	floor.	cab.	bed.	chair.	sofa.	table	door.	wind.	books.	pic.	counter.	desk.	curtain.	fridge.	shower.	toilet.	sink.	bathub.	otherf.
Supervised	PointNet++ [55]	33.9	52.3	67.7	25.6	47.8	36.0	34.6	23.2	26.1	25.2	45.8	11.7	25.0	27.8	24.7	18.3	14.5	54.8	36.4	58.4	18.3
	DGCNN [75]	44.6	72.3	93.7	36.6	62.3	65.1	57.7	44.5	33.0	39.4	46.3	12.6	31.0	34.9	38.9	28.5	22.4	62.5	35.0	47.4	27.1
	PointCNN [36]	45.8	70.9	94.4	32.1	61.1	71.5	54.5	45.6	31.9	47.5	35.6	16.4	29.9	32.8	37.6	21.6	22.9	75.5	48.4	57.7	28.5
	SparseConv [16]	72.5	86.5	95.5	72.1	82.1	86.9	82.3	62.8	61.4	68.3	84.6	32.5	53.3	60.3	75.4	71.0	87.0	93.4	72.4	64.7	57.2
Unsupervised	GrowSP [91]	26.9	32.8	<b>89.6</b>	15.2	62.9	55.3	38.9	32.0	14.4	23.0	<b>59.9</b>	0	12.5	<b>11.4</b>	6.1	<b>1.2</b>	<b>9.3</b>	43.9	<b>14.0</b>	0	16.5
	<b>LogoSP(Ours)</b>	<b>32.7</b>	<b>41.4</b>	87.1	<b>18.1</b>	<b>68.4</b>	<b>56.2</b>	<b>49.9</b>	<b>39.6</b>	<b>30.2</b>	<b>48.7</b>	49.2	<b>0.1</b>	<b>29.1</b>	7.3	<b>33.4</b>	0	0	<b>54.3</b>	0	<b>21.1</b>	<b>19.3</b>

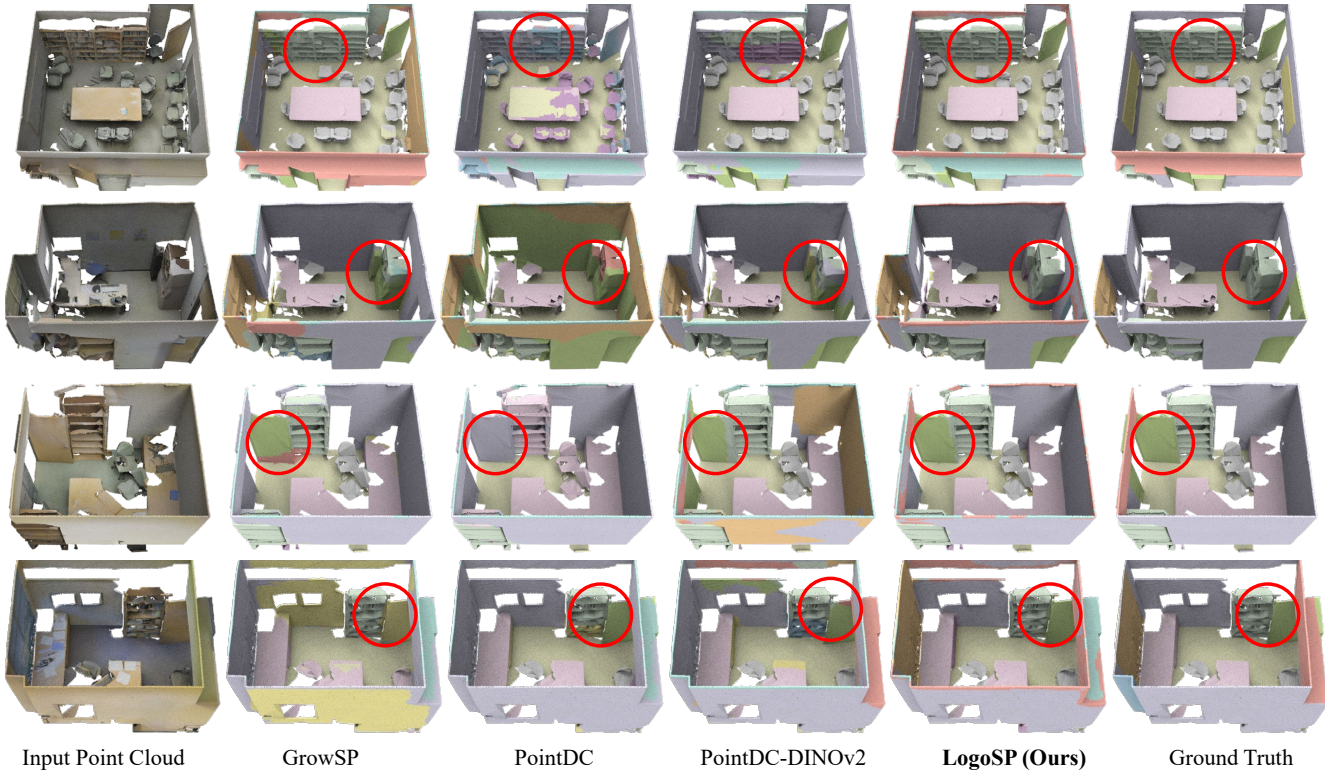


Figure 9. Qualitative results of our method and baselines on the S3DIS dataset.

The per-category results for each area and the 6-fold evaluation are presented in Tables 14 to 20. Our method demonstrates improvements across all areas. Figure 9 shows qualitative results. Since PointDC does not provide detailed results for each category, we reproduce results by training its own models.

## F. Evaluation on nuScenes

After obtaining initial superpoints using RANSAC and Euclidean Clustering, we employ a 15cm voxel grid to convert the point clouds into voxels for training the SparseC-

onv backbone. We also utilize the ViT-S/14 configuration of DINOv2 and maintain the same distillation and segmentation training hyperparameters as used on ScanNet. The training set of nuScenes contains an extremely large number of point clouds, which are challenging to store in memory. Therefore, in each epoch, we randomly select 5,000 point clouds for training; this approach is also applied to all baseline models.

Table 21 shows per-category results, where our model demonstrates superior performance on minor classes like *truck* and *car*. Qualitative results are shown in Figure 10.

Table 14. Quantitative results of our method and baselines on the Area-1 of S3DIS dataset.

		OA(%)	mAcc(%)	mIoU(%)	ceil.	floor	wall	beam	col.	wind.	door	table	chair	sofa	book.	board.
Supervised	PointNet [54]	75.4	74.8	55.0	88.3	93.2	69.2	49.5	37.8	74.5	65.6	41.2	42.5	22.3	35.4	40.9
	PointNet++ [55]	76.1	77.9	58.2	90.5	94.4	65.7	38.2	31.9	61.5	66.0	45.3	60.4	41.2	45.8	57.4
	SparseConv [16]	89.0	79.5	72.5	93.6	95.6	76.1	65.9	60.9	60.0	74.2	81.9	85.4	69.2	73.4	33.5
Unsupervised	Kmeans	20.9	24.1	10.1	15.4	17.8	10.5	16.8	1.9	16.0	12.1	9.9	8.1	0.1	6.2	6.7
	IIC [27]	29.2	14.3	8.0	17.0	31.4	25.6	4.3	11.1	0	2.6	1.4	0.7	0	0.2	1.4
	PICIE [10]	45.7	28.3	19.4	77.2	63.1	24.5	15.8	3.3	4.4	9.6	10.2	14.7	0	9.9	0
	GrowSP [91]	72.9	<b>60.4</b>	45.6	<b>94.2</b>	90.8	52.7	<b>36.7</b>	19.7	33.3	35.8	66.5	<b>72.6</b>	13.1	31.2	<b>16.7</b>
	PointDC [8]	58.0	41.5	28.8	88.7	89.5	31.9	1.5	7.1	17.6	12.4	46.4	17.0	0	32.7	0
	PointDC-DINOV2 [8]	73.8	55.4	44.0	85.7	<b>93.7</b>	58.9	10.1	<b>20.2</b>	0	<b>45.0</b>	<b>70.1</b>	61.5	<b>44.0</b>	39.4	0
	<b>LogoSP (Ours)</b>	<b>76.9</b>	60.0	<b>48.9</b>	89.0	93.2	<b>63.2</b>	27.5	19.2	<b>71.3</b>	39.7	69.7	69.2	0.7	<b>43.6</b>	0

Table 15. Quantitative results of our method and baselines on the Area-2 of S3DIS dataset.

		OA(%)	mAcc(%)	mIoU(%)	ceil.	floor	wall	beam	col.	wind.	door	table	chair	sofa	book.	board.
Supervised	PointNet [54]	72.5	55.5	36.6	79.2	87.4	64.9	14.5	8.2	14.8	39.6	28.8	64.0	7.8	24.4	5.1
	PointNet++ [55]	72.1	62.3	39.9	85.8	69.6	71.2	24.9	27.5	32.5	43.6	27.4	51.3	6.0	26.8	12.4
	SparseConv [16]	87.9	69.5	57.3	89.5	93.8	77.0	29.1	32.5	65.5	45.7	67.9	88.8	34.9	54.5	8.2
Unsupervised	Kmeans	17.6	16.6	6.4	16.4	15.6	11.3	3.3	0.9	0.4	6.8	3.7	11.0	1.4	4.6	1.5
	IIC [27]	41.6	16.8	10.6	33.0	43.7	27.6	1.7	0	0	5.6	0.1	13.0	0	2.8	0
	PICIE [10]	48.3	27.2	17.4	72.4	44.2	39.6	6.2	1.7	0.5	7.7	4.1	20.1	0	7.7	3.6
	GrowSP [91]	<b>79.0</b>	51.8	39.1	85.7	88.2	67.0	<b>12.0</b>	<b>24.8</b>	0	24.2	51.2	77.1	<b>4.1</b>	24.5	0.2
	PointDC [8]	48.3	34.8	22.5	66.7	50.2	26.1	1.3	0.4	0	15.6	29.8	56.3	0.3	17.6	<b>5.6</b>
	PointDC-DINOV2 [8]	77.1	50.3	38.1	90.8	<b>92.0</b>	57.3	10.2	0.6	34.2	20.3	46.4	<b>85.6</b>	0	19.1	0.9
	<b>LogoSP (Ours)</b>	77.0	<b>52.2</b>	<b>39.4</b>	<b>92.3</b>	67.7	<b>72.0</b>	7.2	0.7	<b>44.8</b>	<b>32.4</b>	<b>58.0</b>	53.3	0.2	<b>44.1</b>	0.5

Table 16. Quantitative results of our method and baselines on the Area-3 of S3DIS dataset.

		OA(%)	mAcc(%)	mIoU(%)	ceil.	floor	wall	beam	col.	wind.	door	table	chair	sofa	book.	board.
Supervised	PointNet [54]	78.2	74.9	57.7	90.3	96.9	66.9	55.5	15.1	60.0	67.7	51.8	54.8	27.6	56.0	50.0
	PointNet++ [55]	79.8	85.9	65.8	91.4	98.0	68.5	50.1	15.2	74.8	74.7	63.2	70.1	53.6	54.0	76.5
	SparseConv [16]	91.3	86.8	78.6	93.1	96.2	80.4	74.7	63.3	77.2	69.5	80.1	85.5	89.5	80.1	52.5
Unsupervised	Kmeans	21.3	22.1	9.4	20.2	20.6	13.3	5.7	1.3	2.3	14.1	6.8	6.8	3.7	9.7	8.6
	IIC [27]	32.1	15.4	8.4	20.5	25.5	31.4	1.0	6.9	0.2	3.2	1.6	0.3	0	10.6	0
	PICIE [10]	40.4	29.2	16.2	50.5	49.6	33.7	13.2	3.0	1.8	6.5	8.9	7.5	3.5	16.2	0.4
	GrowSP [91]	74.2	<b>68.4</b>	47.7	<b>92.9</b>	91.7	48.3	<b>49.3</b>	15.8	21.1	38.7	60.6	<b>66.5</b>	<b>28.5</b>	59.2	0
	PointDC [8]	56.2	40.7	27.2	75.3	91.3	29.7	1.2	2.2	0	11.4	37.9	20.7	9.2	38.4	<b>8.9</b>
	PointDC-DINOV2 [8]	70.5	52.4	39.3	86.2	93.4	48.8	0	14.5	38.6	28.2	<b>68.7</b>	55.0	0	37.7	0
	<b>LogoSP (Ours)</b>	<b>79.8</b>	62.7	<b>48.9</b>	90.0	<b>94.3</b>	<b>65.9</b>	16.0	<b>18.6</b>	<b>67.8</b>	<b>45.5</b>	59.2	56.3	3.6	<b>69.4</b>	0

Table 17. Quantitative results of our method and baselines on the Area-4 of S3DIS dataset.

		OA(%)	mAcc(%)	mIoU(%)	ceil.	floor	wall	beam	col.	wind.	door	table	chair	sofa	book.	board.
Supervised	PointNet [54]	73.0	58.6	41.6	81.3	95.7	68.4	1.3	22.4	29.0	44.8	39.3	42.5	17.6	36.6	20.1
	PointNet++ [55]	74.8	66.4	47.7	85.5	96.1	69.9	4.4	23.8	27.0	50.5	44.9	54.0	35.6	38.4	43.8
	SparseConv [16]	88.3	76.2	65.5	93.0	94.9	78.2	53.3	57.9	43.4	59.1	69.4	76.6	55.1	73.8	30.9
Unsupervised	Kmeans	17.9	19.9	7.8	18.6	18.2	10.6	0.9	3.8	5.2	11.7	5.8	7.4	2.4	8.7	0.4
	IIC [27]	33.0	13.5	8.2	14.9	25.9	35.1	0	1.1	1.4	3.7	4.1	0.9	0	10.8	0
	PICIE [10]	43.2	29.4	17.8	62.2	72.7	22.6	2.5	3.4	3.5	8.8	4.1	17.4	0	15.5	0.7
	GrowSP [91]	76.0	<b>59.8</b>	42.8	90.6	91.5	64.4	<b>15.9</b>	<b>7.6</b>	27.4	31.5	52.0	<b>67.4</b>	16.8	48.5	0
	PointDC [8]	54.0	35.3	25.2	87.9	86.8	24.7	0	4.2	12.2	18.7	32.6	17.6	1.9	15.6	0
	PointDC-DINOV2 [8]	73.0	46.5	39.8	89.4	91.9	58.2	0	0.7	25.3	19.0	52.4	53.8	0.7	59.0	0
	<b>LogoSP (Ours)</b>	<b>80.8</b>	54.4	<b>43.5</b>	<b>92.5</b>	<b>93.8</b>	<b>73.9</b>	4.1	0.1	<b>34.8</b>	<b>44.6</b>	<b>54.0</b>	64.9	<b>69.2</b>	<b>73.4</b>	<b>33.5</b>

In addition to the experiments conducted on the validation set of nuScenes, we present segmentation results on its online hidden test set. This test set comprises 6008 outdoor point clouds categorized into 16 classes. Since there is no other unsupervised baseline evaluated on the hidden test set, we include successful fully-supervised methods for comparison. All models listed in Table 22 are trained us-

ing the training set of nuScenes and then evaluated on the hidden test set. These results demonstrate the promising effectiveness of our unsupervised segmentation model.

Table 18. Quantitative results of our method and baselines on the Area-5 of S3DIS dataset.

		OA(%)	mAcc(%)	mIoU(%)	ceil.	floor	wall	beam	col.	wind.	door	table	chair	sofa	book.	board.
Supervised	PointNet [54]	77.5	59.1	44.6	85.2	97.4	72.3	0.1	10.6	54.9	18.5	48.4	39.5	12.4	55.5	40.2
	PointNet++ [55]	77.5	62.6	50.1	83.1	97.2	66.4	0	8.1	55.6	15.2	60.4	64.5	36.6	58.3	55.7
	SparseConv [16]	88.4	69.2	60.8	92.6	95.9	77.2	0.1	36.7	37.6	59.8	77.2	83.9	59.7	78.5	30.4
Unsupervised	Kmeans	21.4	21.2	8.7	18.7	18.0	16.7	<b>0.2</b>	2.5	12.0	5.7	8.7	5.6	0	13.6	<b>2.3</b>
	IIC [27]	28.5	12.5	6.4	6.1	19.8	27.9	0	2.1	0.1	3.4	7.9	0.4	0	8.6	0
	PICIE [10]	61.6	25.8	17.9	65.7	61.4	58.4	0	0.3	2.2	1.7	12.1	0	0	12.4	0
	GrowSP [91]	78.4	<b>57.2</b>	44.5	90.5	90.1	66.7	0	<b>14.8</b>	27.6	<b>45.6</b>	59.4	71.9	<b>10.7</b>	56.0	0.2
	PointDC [8]	55.5	35.1	23.9	84.4	84.3	30.2	0	1.8	12.2	7.1	24.6	6.9	5.4	29.7	0.7
	PointDC-DINOv2 [8]	75.7	48.7	40.2	87.7	89.5	59.2	0	0.8	25.8	26.3	<b>62.0</b>	68.3	1.5	61.0	0.5
	<b>LogoSP (Ours)</b>	<b>82.8</b>	55.9	<b>46.5</b>	<b>92.9</b>	<b>95.4</b>	<b>73.2</b>	0	3.3	<b>57.8</b>	35.9	55.5	<b>74.6</b>	1.9	<b>67.3</b>	0.3

Table 19. Quantitative results of our method and baselines on the Area-6 of S3DIS dataset.

		OA(%)	mAcc(%)	mIoU(%)	ceil.	floor	wall	beam	col.	wind.	door	table	chair	sofa	book.	board.
Supervised	PointNet [54]	79.0	79.6	60.9	85.7	96.5	71.8	59.4	47.4	67.4	74.3	56.2	48.9	20.9	50.0	52.5
	PointNet++ [55]	82.0	89.3	69.0	87.5	96.3	76.8	66.4	54.4	72.1	77.4	64.3	66.5	43.7	51.8	70.2
	SparseConv [16]	91.6	87.3	80.5	97.4	95.0	83.4	83.0	75.1	81.1	74.9	81.3	84.3	79.0	80.7	61.4
Unsupervised	Kmeans	21.0	25.0	10.4	18.6	17.6	8.9	11.3	0.6	14.8	17.6	12.0	8.7	0.3	7.8	<b>6.2</b>
	IIC [27]	32.5	15.9	9.2	21.9	33.8	29.1	3.1	15.2	0	2.7	0.7	0	0	1.5	1.8
	PICIE [10]	39.3	28.5	17.8	56.9	61.7	18.6	20.5	4.2	6.0	8.7	14.7	15.9	1.1	5.7	0
	GrowSP [91]	75.6	58.5	47.6	89.4	88.0	57.7	<b>70.6</b>	2.0	32.4	36.7	63.2	69.8	1.5	58.9	0.2
	PointDC [8]	62.4	38.7	28.6	85.8	85.6	43.8	5.0	16.5	8.8	10.7	41.7	12.5	0	33.0	0
	PointDC-DINOv2 [8]	76.4	55.5	46.4	<b>90.3</b>	91.4	61.7	0	19.7	63.1	33.6	67.9	65.7	1.4	62.5	0
	<b>LogoSP (Ours)</b>	<b>77.9</b>	<b>62.9</b>	<b>50.6</b>	84.6	<b>92.7</b>	<b>64.0</b>	25.7	<b>23.9</b>	<b>65.9</b>	<b>38.8</b>	<b>68.9</b>	<b>72.2</b>	<b>2.5</b>	<b>68.4</b>	0

Table 20. Quantitative results of our method and baselines on the 6-fold validation on S3DIS dataset.

		OA(%)	mAcc(%)	mIoU(%)	ceil.	floor	wall	beam	col.	wind.	door	table	chair	sofa	book.	board.
Supervised	PointNet [54]	75.9	67.1	49.4	85.0	94.5	68.9	30.0	23.6	50.1	51.8	44.3	48.7	18.1	43.0	34.8
	PointNet++ [55]	77.1	74.1	55.1	85.7	91.6	69.8	36.0	28.0	58.7	57.4	47.4	61.8	39.1	44.1	61.2
	SparseConv [16]	89.4	78.1	69.2	94.6	95.5	78.6	51.8	55.8	60.6	63.0	76.0	84.3	65.8	73.5	39.4
Unsupervised	Kmeans	20.0	21.5	8.8	17.9	17.9	11.6	6.5	1.8	8.2	11.1	7.9	7.9	1.5	8.4	4.8
	IIC [27]	32.8	14.7	8.5	18.9	30.0	29.3	1.7	7.2	0.4	3.4	2.8	2.5	0	5.5	0.6
	PICIE [10]	46.4	28.1	17.8	63.6	58.6	33.3	9.0	2.6	3.2	7.6	9.7	12.4	0.9	11.5	0.9
	GrowSP [91]	76.0	<b>59.4</b>	44.6	<b>90.7</b>	89.9	60.2	<b>30.6</b>	<b>14.9</b>	24.0	35.6	58.4	<b>70.6</b>	12.5	44.9	3.5
	PointDC [8]	55.7	37.7	26.0	81.5	81.5	31.4	1.5	6.4	8.8	12.2	35.8	20.8	2.6	27.5	2.4
	PointDC-DINOv2 [8]	74.4	51.5	41.3	88.8	<b>91.8</b>	57.9	3.4	10.4	27.5	28.3	<b>61.3</b>	64.8	<b>13.8</b>	43.9	0.3
	<b>LogoSP (Ours)</b>	<b>79.2</b>	58.0	<b>46.3</b>	90.2	89.5	<b>68.7</b>	13.4	10.9	<b>57.1</b>	<b>39.5</b>	60.9	65.1	13.0	<b>60.4</b>	<b>5.7</b>

Table 21. Per-category quantitative results on the validation split of nuScenes dataset.

	OA(%)	mAcc(%)	mIoU(%)	barrier.	bicycle.	bus.	car.	construction vehicle.	motorcycle.	pedestrian	traffic cone.	trailer.	truck.	drivable surface.	other flat.	sidewalk.	terrain.	manmade.	vegetation.
GrowSP [91]	39.2	17.5	10.2	7.5	0	0.4	42.9	0.1	0	0.6	0	0.7	1.4	48.4	<b>0.8</b>	6.5	13.1	21.4	19.7
PointDC [8]	<b>56.8</b>	<b>29.4</b>	17.7	11.6	0	0.5	63.1	<b>0.3</b>	0	4.4	0	1.2	26.4	70.1	0.1	7.1	19.3	21.1	<b>58.1</b>
PointDC-DINOv2 [8]	51.8	28.6	18.2	<b>17.0</b>	0	0.2	58.4	0.2	0	1.5	0	<b>1.6</b>	<b>43.3</b>	<b>71.8</b>	0	<b>8.3</b>	<b>19.5</b>	17.6	51.8
<b>LogoSP (Ours)</b>	54.8	29.2	<b>20.1</b>	16.6	0	<b>0.7</b>	<b>70.2</b>	0.2	<b>0.2</b>	<b>33.6</b>	0	0.3	38.4	59.4	0.4	8.0	10.7	<b>33.0</b>	49.3

Table 22. Per-category quantitative results on the **hidden test split** of nuScenes dataset.

		mIoU(%)	barrier.	bicycle.	bus.	car.	construction vehicle.	motorcycle.	pedestrian.	traffic cone.	trailer.	truck.	driveable.	other flat.	sidewalk.	terrain.	manmade.	vegetation.
Supervised	Cylinder3D [95]	77.2	82.8	29.8	84.3	89.4	63.0	79.3	77.2	73.4	84.6	69.1	97.7	70.2	80.3	75.5	90.4	87.6
	SPVNAS [68]	77.4	80.0	30.0	91.9	90.8	64.7	79.0	75.6	70.9	81.0	74.6	97.4	69.2	80.0	76.1	89.3	87.1
	Cylinder3D++ [95]	77.9	82.8	33.9	84.3	89.4	69.6	79.4	77.3	73.4	84.6	69.4	97.7	70.2	80.3	75.5	90.4	87.6
Unsupervised	<b>LogoSP(Ours)</b>	17.5	12.4	0	1.9	68.7	0	0.2	22.5	0	0.1	23.2	62.8	0.2	1.4	13.9	30.1	41.6



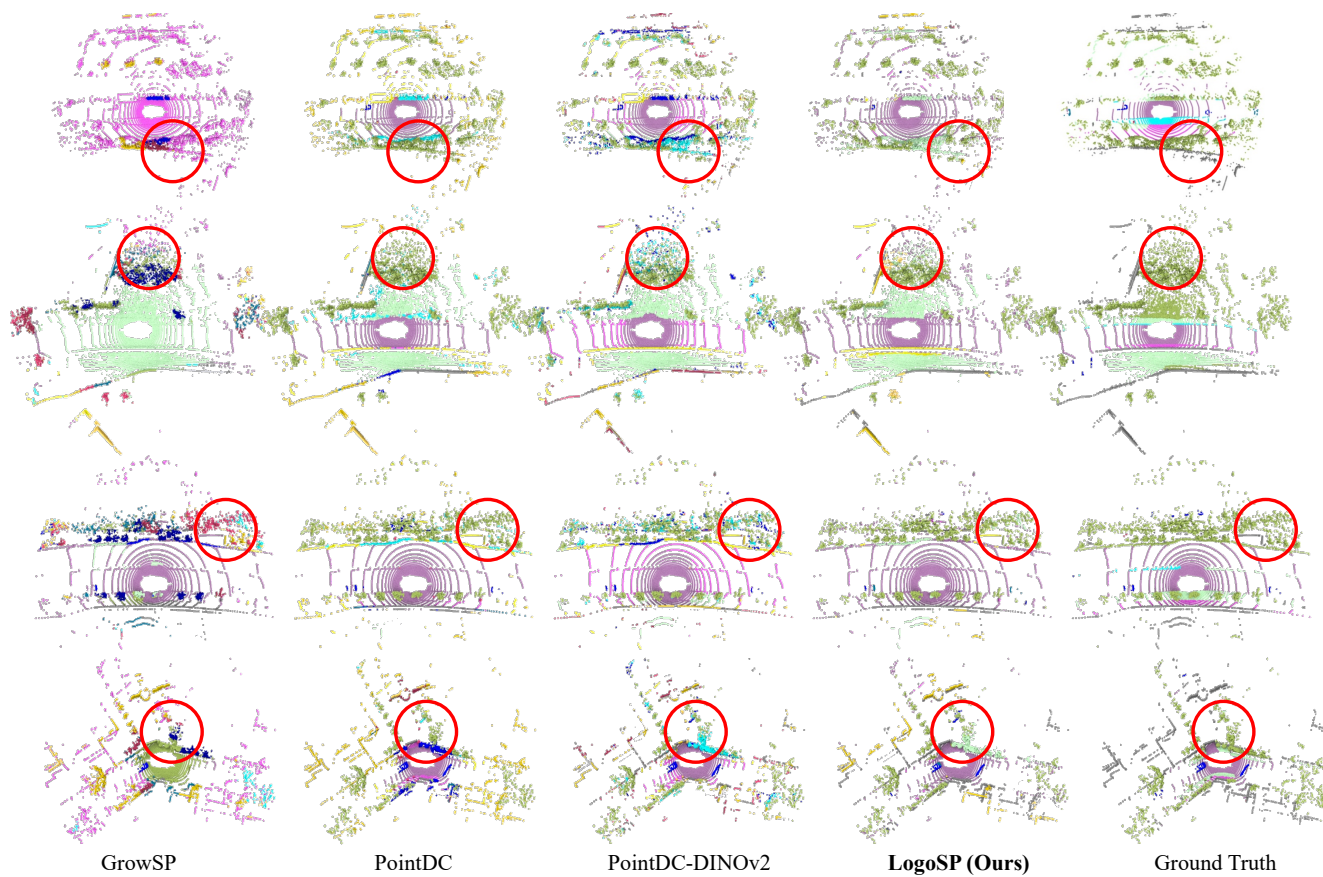


Figure 10. Qualitative results of our method and baselines on the nuScenes dataset.